Manganese oxide, Iron oxide Magnetic Clay Composite for the Detection of Chromium from Solution

By

Amnah Jaral

School of Chemical and Materials Engineering (SCME)

National University of Science and Technology (NUST)

2018

Manganese oxide, Iron oxide Magnetic Clay Composite for the Detection of Hexavalent Chromium from Solution

Name: Amnah Jaral

Reg. No: 00000119715

This thesis is submitted as a partial fulfilment of the requirement for the degree of MS in Nano science and Engineering

Supervisor: Dr. Zakir Hussain

School of chemical and Materials Engineering (SCME)

National University of Science and Technology (NUST), H-12

Islamabad, Pakistan

April 2018

Certificate

This is to certify that work in this thesis has been carried out by **Miss Amnah Jaral** and completed under my supervision at School of Chemical and Materials Engineering, National University of Sciences and Technology, H-12, Islamabad, Pakistan.

Supervisor**:** _____

Prof. Dr. Zakir Hussain

Materials Engineering Department

National University of Sciences and

Technology, Islamabad

Submitted through

Principal/Dean,

School of Chemical and Materials Engineering Department

National University of Sciences and Technology, Islamabad

Dedication

I would like to dedicate my beloved parents, friends and my supervisor. I couldn’t be able to achieve this milestone without them. It is their love, support and guidance which keep me motivated and ambitious to fulfill my dreams. I am nothing without them. This work is sign of my love to them.

Acknowledgements

"Truly my prayer and my service of sacrifice, my life and my death, are (all) for ALLA**H**, the Rabb of worlds".

It is my privileged to express appreciation and gratitude to my research supervisor, **Dr. Zakir Hussain**, for his constant support, advice, valuable comments, constant persuasion and efficient supervision at every stage of research work. I am really thankful to my committee members **Dr. Iftikhar Hussain Gul** and **Dr. Umair Manzoor** whose remarkable suggestions, constructive criticism and guidance during my project, without their support, this could not have been possible.

I acknowledge **Prof Dr. Mohammad Arshad (Principal, SCME), Prof Dr. Umair Manzoor (HOD, SCME),** all faculty members, lab engineers, lab technical staff and non-teaching staff.

Ialso acknowledge all my fellows and friends for their help at various stages during this research work

Amnah Jaral

Abstract

In this work, an efficient adsorbent for the removal of chromium (IV) was prepared. The examined heavy metal adsorbents are Fe_3O_4 and MnO_2 nanoparticles, nanoclay, Fe_3O_4/Clay and MnO_2/Fe_3O_4/Clay nanocomposites. The MnO_2/Fe_3O_4/Clay nanocomposite is used for the first time for detection of heavy metal ions. The adsorption studies showed that nanoparticles have very low removal efficiency whereas Fe_3O_4/clay composite showed better removal of toxic metal ions. The maximum removal was observed for MnO_2/Fe_3O_4/Clay nanocomposite. The maximum adsorption capacity of MnO_2/Fe_3O_4/Clay nanocomposite was calculated as 384 mg/g which is the highest among all the used adsorbents. The reported adsorption capacity is higher than the previously reposted adsorbent capacities for chromium. During the synthesis of MNO_2/Fe_3O_4/Clay nanocomposite, Fe_3O_4 and MnO_2 nanoparticles are efficiently assembled over the surface of nanoclay (Cloisite 30-B). MnO_2/Fe_3O_4/Clay nanocomposite was found to be more effective for the removal of chromium (cr^{6+}) ions via adsorption process where the adsorption was found to be strongly dependent on the initial pH of the solution. The maximum adsorption capacity was calculated to be 384 mg/g. Contact time and kinetics of adsorption confirmed that the process can be explained by pseudo second order rate equation. Obtained results demonstrate that MnO_2/Fe_3O_4/Clay nanocomposite could be exploited as a promising material for the efficient removal of chromium from wastewater.

The morphology, chemical, optical and structural properties of nanoparticles, nanoclay and nanocomposite were studied using Scanning electron microscopy (SEM), Fourier transform infrared (FTIR) spectroscopy, ultra-violet visible (UV-Vis) spectroscopy and X-ray diffraction (XRD). SEM showed that the prepared nanoparticles are uniformly dispersed over the clay surface, without any agglomeration. FTIR analysis confirmed the various bonds within the clay structure along with the metal oxide bonds of nanoparticles. The peak position and intensity confirmed the physical assembling of nanoparticles on clay. XRD showed the corresponding peaks of MnO_2/Fe_3O_4/Clay nanocomposite.

Contents

List of Figures

List of Tables

List of Abbreviations

Meaning	Acronym
Heavy metal ions	HMI
Manganese oxide	MnO_2
Iron oxide	Fe_3O_4
Nanoparticles	NPs
Nanocomposite	NCs
Montmorillonite	MMT
X-Ray diffraction	XRD
Scanning Electron Microscopy	SEM
Ultra-violet Spectroscopy	UV-V is spectroscopy
Fourier Transform infrared	FTIR
Adsorption capacity at equilibrium	q_e
Chromate ion	Cr^{6+}
Solute concentration at equilibrium	C_e

Chapter 1

Introduction

Any element whether it is metal or metalloid consider to be “heavy metal” having larger density lying within the range of 3.5 to 7 g cm^{-3} and specific gravity higher than 5.0. These elements are poisonous and hazardous even at minimum concentrations. Generally, the term heavy metal is used to represent the hazardous and widespread toxic specie in soil and aqueous system. Among heavy metals, mercury (Hg), cadmium (Cd), arsenic (As), chromium (Cr), thallium (Tl), zinc (Zn), nickel (Ni), copper (Cu) and lead (Pb) are most toxic and have adverse effect on environment [1, 2, 3]. Little amount of these chemical is required for continuation of life cycle, cell signaling and have significant part in metabolic activity of living organism. But their concentrations have some severe impacts on ecosystem. Naturally, these metals exist in the, rocks soil and earth crust but their concentration is increasing rapidly due to human activities [4]. Utilization of metal salts and derivatives or different compounds of heavy metals in different applications because of their wider chemical properties and promising results, has raised their concentration level and their accumulation in the environment. They enter and accumulate into the ecosystem due to, mining, industrial effluent, house old applications, naturally occurring geochemical weathering phenomenon of soil, rocks and landfill leaches. Fig. 1.1 shows the release of toxic metals into environment due to human activities.

Accumulation of such metals creating problems for human and other living system. Contrary to organic pollutants, heavy metals have non-biodegradable nature and remain in the environment for undefined time. Their solubility, mobility in the water and ability to cross cell walls affects biochemical activities, made them really threating for life cycles. They are soluble in the aquatic system so their mobility can’t be controlled easily. They can enter in to living organism by alimentary chains. They interact chemically with other protein sites hence lead to hazards in aquatic biota, humans, plants and animals. Their chemical interference inhibits the enzymatic

activity, generation of free radicals, loss of protein and induces oxidative stress thereby disturbing living organism's health [4].

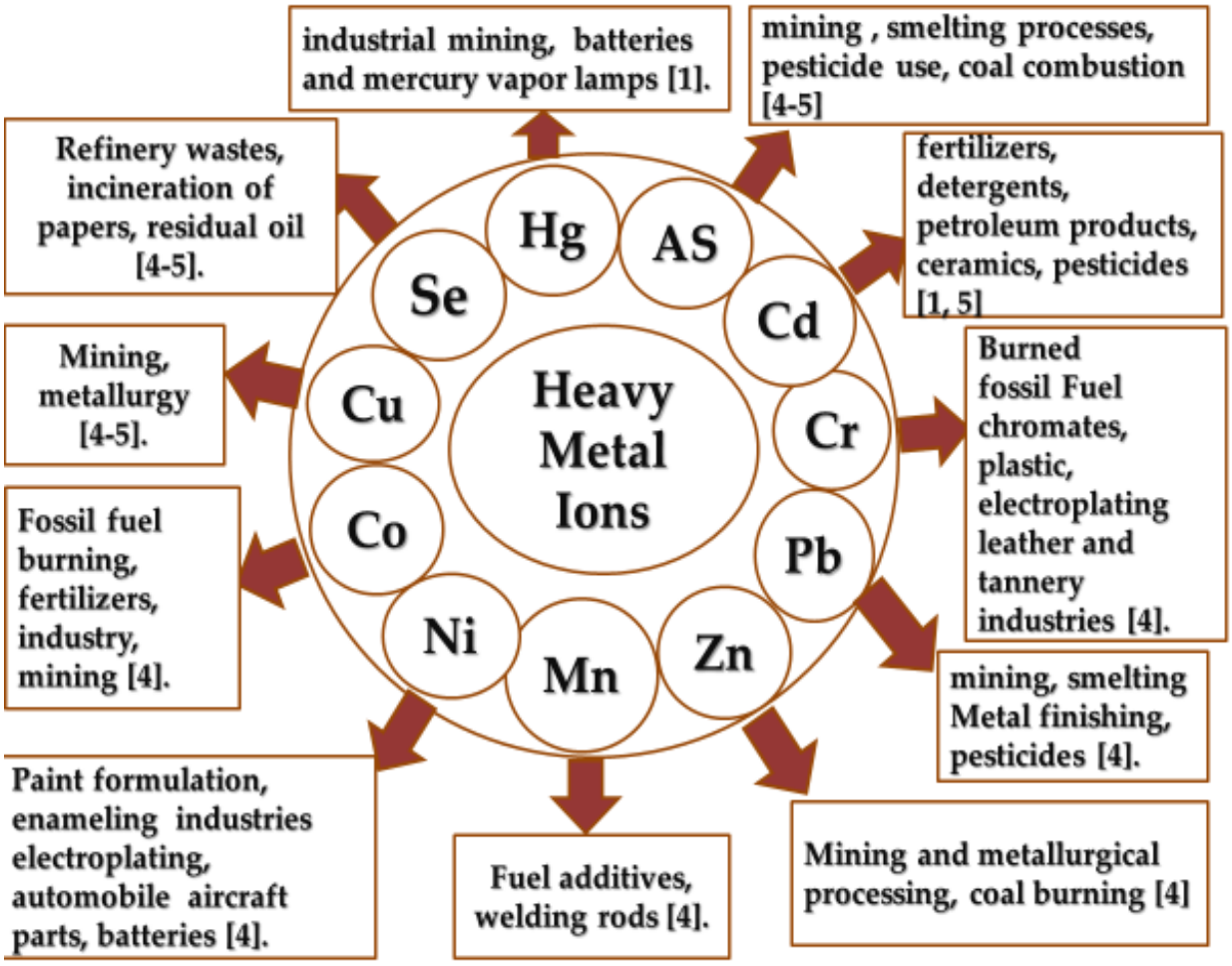

Fig.1.1: Anthropogenic sources of metals

To regulate the concentration of these heavy metal ions and their toxicity, several international organizations mainly, World Health Organization (WHO), Centre for Disease Control (CDC), Joint Food and Agricultural Organization (FAO)/WHO Expert Committee on Food, Additives (JECFA), and International Agency for Research on Cancer (IARC) are working and defining the optimum concentration of these metal ion in the water soli or food, that is not armful for human beings [3].

Lead causes metabolic poisons, tiredness anemia and behavioral changes of children's. Its exposure leads to hallucination, hypertension, brain damage insomnia, also causes phytotoxicity. Damages renal and reproductive system, basic cellular functioning, liver and brain. According to environmental protection agency the maximum concentration of lead in water must be less ten 0.1mg/L. presence nickel metal in living organisms directly effects DNA, gastrointestinal distress and in most cases, it causes the DNA mutation, respiratory and renal issues, pulmonary fibrosis. Eczema of hands, severe phytotoxicity, infected fauna and skin dermatitis are the effects of nickel metal. Its maximum allowed concentration in the aqueous system and drinking water is 0.1mg/l. Mucosal irritation, corrosion of systems, irritation of nervous system, cramps, convulsions, sometimes even death and respiratory problems are linked with the exposure to accumulation of copper with in human body. EPA defined 1.0 mg/L as its maximum concentration in drinking water.

Zinc has phytotoxic effects, causes eminent health problems mainly stomach cramps, nausea, vomiting skin irritations, anemia, diminishes the muscular coordination, effects motor neurons and mostly abdominal pain. Its maximum allowed concentration in aqueous system is 5mg/l. Cadmium has adverse effect on kidney, bones causes bronchitis, anemia, acute renal failure and acute effects in babies. According to EPA it must be less than 0.0005 mg/L. Mercury is highly carcinogenic and poisonous metal having mutagenic effects and creates cholesterol disturbance, dyspnea. Its optimum limit in drinking water is 0.002m/l. Arsenic have also carcinogenic effects, causes melanosis, keratosis and hyperpigmentation in humans, endotoxicity through generation of reactive species and immunotoxicity are the outcomes of arsenic exposure [1].

Chromium usually exists in oxidation states ranges from (II-IV) but in aqueous system chromium has only two stable states such as hexavalent [Cr(VI)] along with trivalent [Cr(III)]. Cr(III) is less toxic and essential for metabolic activities of human beings. Accumulation of Cr(III) up to certain level can cause severe problems but Cr(IV) is extremely toxic even at low concentration level [7]. Exposure to chromium(IV) leads to damage of testicular tissue, changes in metabolic path because of their production of cholesterol, mutagenic effects, steroidogenesis, lung carcinoma, genomic, inflammation and in severe cases, tumor of respiratory pathway, instability, cell membrane damage, skin irritation, gastrointestinal ulcers and immune deficiency,

respectively. For safety measures the maximum concentration of chromium in aqueous system must be less than 100 μG L^{-1} [1, 3, 8].

In case of the presence of these metals higher than the defined level, detection of such metal ions is mandatory. Numerous removal processes are defined and used for long period of time. The most commonly used methods are cyanides [9], electrochemical precipitation [2], adsorption [10], electrochemical sensors [10], colorimetric detection [11] flotation and ultrasonic-assisted extraction [2]. Cyanide technique generates highly toxic products during the reaction, which have adverse effects on environment, precipitation has large volume sludge removal issues. Focusing on the initial concentration of metal and sensing material, the byproducts of the treatment, capital investment, component of waste, operational cost, experimental flexibility and environmental influence, adsorption is the most effective and favorable process for the removal and the detection of metal ions. As it offers the removal of toxic metals at nanoscale, greater efficiency even at low concentration of adsorbent. Several adsorbents have been utilized for the treatment of aqueous system such as activated carbon, clay minerals, graphene, graphene oxide, carbon natures, conducting polymers and many different composites [12, 13, 14]. Although, carbon family is frequently used for the polluted water treatment but for wide range of applications and preparation of nanocomposite, aluminosilicate family (clays) offers larger opportunities. Former structures have less efficiency at lower concentrations of pollutants up to trace levels [15]. Nanostructures of iron and manganese and their oxide have been recognized as much favorable materials for the retention of heavy metals [16-20]. Several morphologies of both nanoparticles such as rods, tubes, porous structures, films, wires and spheres have been utilized for the pollutants remediation from the contaminated water. Using both nanostructures at the same time for removal of metals offers larger efficiency because of their large surface area alongwith magnetic attributes of magnetic properties [14, 9].

1.1. Stratification of magnetic materials:

The difference in the response of material when placed in a magnetic field can be due to several factors mainly atomic / molecular structure or magnetic moment of atoms. The spin and orbital moment of electrons significantly influence the magnetic moment and change accordingly by

externally applied magnetic field. Some magnetic materials align parallel to applied fielded some opposite to it. This is basically linked with spinning of paired or unpaired electrons [18].

The magnetic response can be categorized as follows:

1. Para magnetism
2. Diamagnetism
3. Ferro/Ferrimagnetism
4. Super-Para magnetism
5. Antiferromagnetic

1.1.1 Para magnetism:

The Paramagnetic behavior is due to the orbital and spin magnetic moment which are not completely canceled out. In the presences of magnetic field, the randomly oriented dipole moments get aligned in the direction of field and this will end up higher net magnetization.

1.1.2. Diamagnetism:

The overall magnetic moment of material is zero in the presences of magnetic field. Orbital moment of electrons originates in a manner which generates magnetic field in totally opposite to applied magnetic field and give rise to diamagnetism. In this case material tends to move in the direction where magnetic field is weak.

1.1.3. Ferromagnetism and ferrimagnetism:

The material having some permanent magnetization without applying external magnetic field are considered as ferromagnetic and ferrimagnetic materials. Such materials have larger value of permanent magnetization. Atomic spins and interactions with neighboring atoms is in such a way that alignment of all spins have same direction.

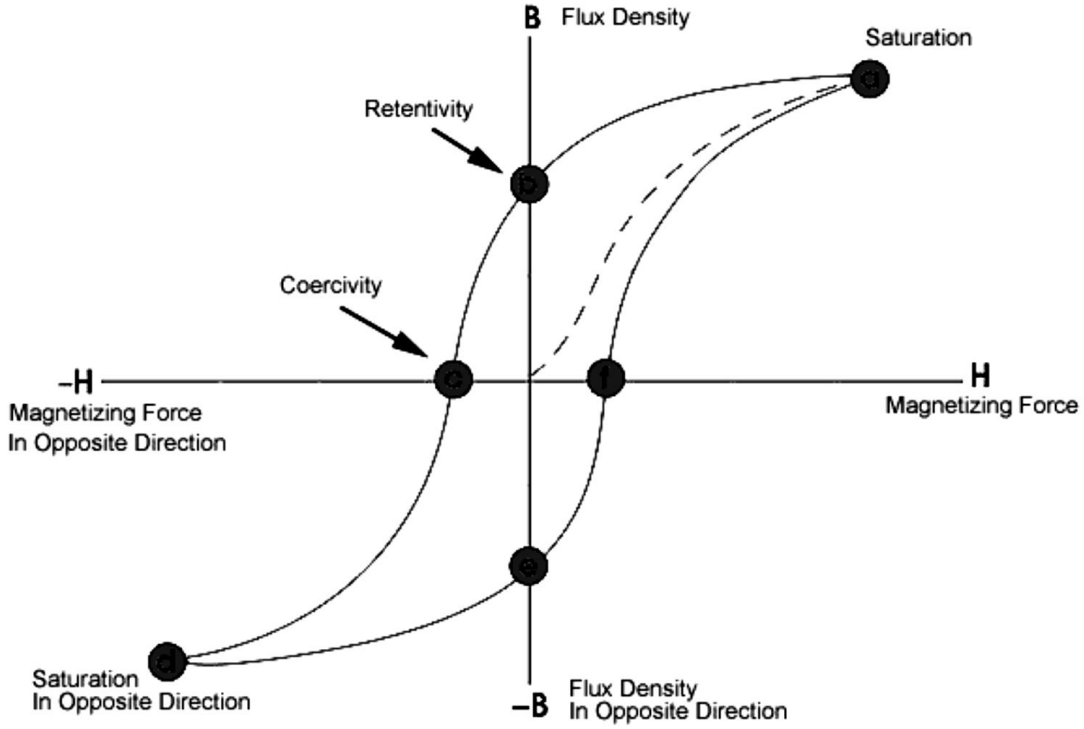

Fig.1.2: Response of Ferromagnetic material in externally applied field [17].

1.1.4. Anti-ferromagnetism:

The magnetic moments aligned in a pattern to the moment of neighboring atoms oriented in opposite direction resulting in anti-ferromagnetism. This behavior is observable at very low temperature named as Neel temperature, and vanishes above neel temperature [18, 19].

1.2. Ferrites:

The ferromagnetic materials have ferrite (component of iron oxide) as their important element. The presence of such ferromagnetic oxides leads to their insulating nature. Depending upon hysteresis losses, ferrites are classified as i). hexagonal and ii) cubic structure.

Generally, ferrites are classified in to three groups depending on the structure, as follows:

Garnet ferrites (M_3Fe5O_{12}): have a cubic structure. Whereas M is trivalent ion of rare earth metal (Y, Dy, Gd). They are also known as hard materials.

Spinal ferrites (MFe_2O_4): While M is divalent cations (Ni^{2+}, Co^{2+}, Fe^{2+}). They have Relatively simple structure. 32 oxygen ions are in unit cell 32. Anions have face centered cubic closed packed arrangements in the structure. The unit cell has two sites A and B within anions, referred as tetrahedral and octahedral sites correspondingly. The 4 oxygen atoms surround a tetrahedral site. There are 64 tetrahedral and 32 octahedral sites in a structure. The cations are on 8 tetrahedral sites and 6 oxygen atoms surrounding an octahedral site. The anions are on 16 octahedral sites. These structures are electrically neutral because of presence of tetrahedral and octahedral sites.

There are two types of spinel structure:

(a) Inverse spinel: In a lattice, trivalent ions are on both tetrahedral and octahedral sites while divalent ions are on octahedral sites.

(b) Normal spinel: In a lattice, the divalent metal ions have tetrahedral site and trivalent metal ions occupy octahedral sites.

Hexagonal ferrites ($MFe_{12}O_{19}$); Where M (barium, cobalt, strontium etc. or their combination). They are considered as permanent magnets. Three occupied sites by metal are tetrahedral, octahedral and trigonal.

1.3. MnO_2 Nanostructures:

Among the chemically active nonprecious oxides (metal oxides), MnO_2 is presently considered as most effective material. Metal oxide crystallizes into five polymorphs due to the bonding of fundamental MnO_6 octahedral unit, depending on the bonding motifs they have tunneled or

interlayered structure with varying gaps. These crystallographic structures are named as, R, α, β, δ, and λ structures. α-MnO_2 comprises Cryptomelane-type structure, having (1x2) and (2x2) channels in c-axis. In this structure edge chains shared double octahedra with adjacent chains. The λ-MnO_2 polymorph, is not naturally existing structure, is product of cycling of lithium $LiMn_2O_4$, and exhibits the spinel framework. According to the reported literature synthetic polymorph λ-MnO_2 and α-MnO_2 material are considered as active materials for their utilization as catalyst and electrochemical studies.

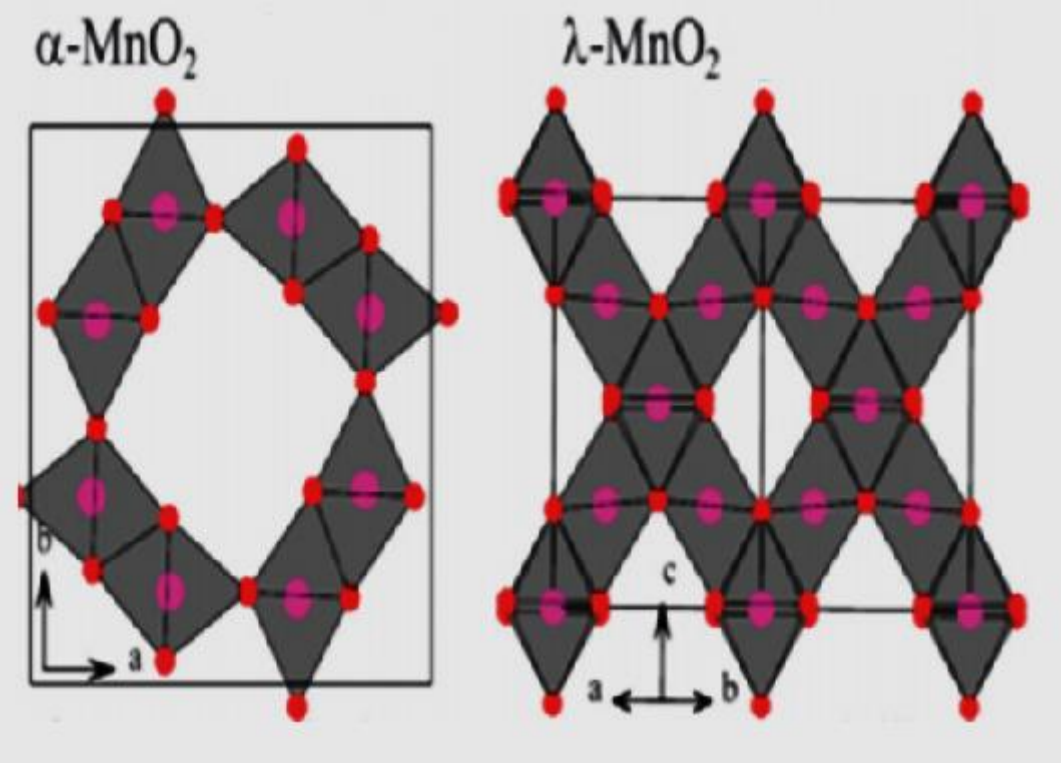

Fig. 1.3: Crystallographic Structure of MnO_2 polymorphs; **a)** α-MnO_2 and **b)** λ-MnO_2 [22].

1.4. Nanoclays:

Platy structured, clay minerals are the fundamental elements of clay raw materials. The clay minerals are largely classified depending upon the amount and arrangement of packing of tetrahedral $[SiO_4]^{4-}$ and octahedral $[AlO_3(OH)_3]^{6+}$ sheets within clay. Such aluminosilicate

layers arrange themselves above one another with an even van der Waals gap with in layers known as 'interlayer'. Interlayer have negative charge because of ionic substitutions within the clay sheets and neutralized using charges reside in the inter-lamellar. These cations can be substituted by other cations, molecules or compounds according to surface chemistry these exchangeable cations are Na^{+}, K^{+}, Mg^{2+}, and Ca^{2+} in the interlayer.

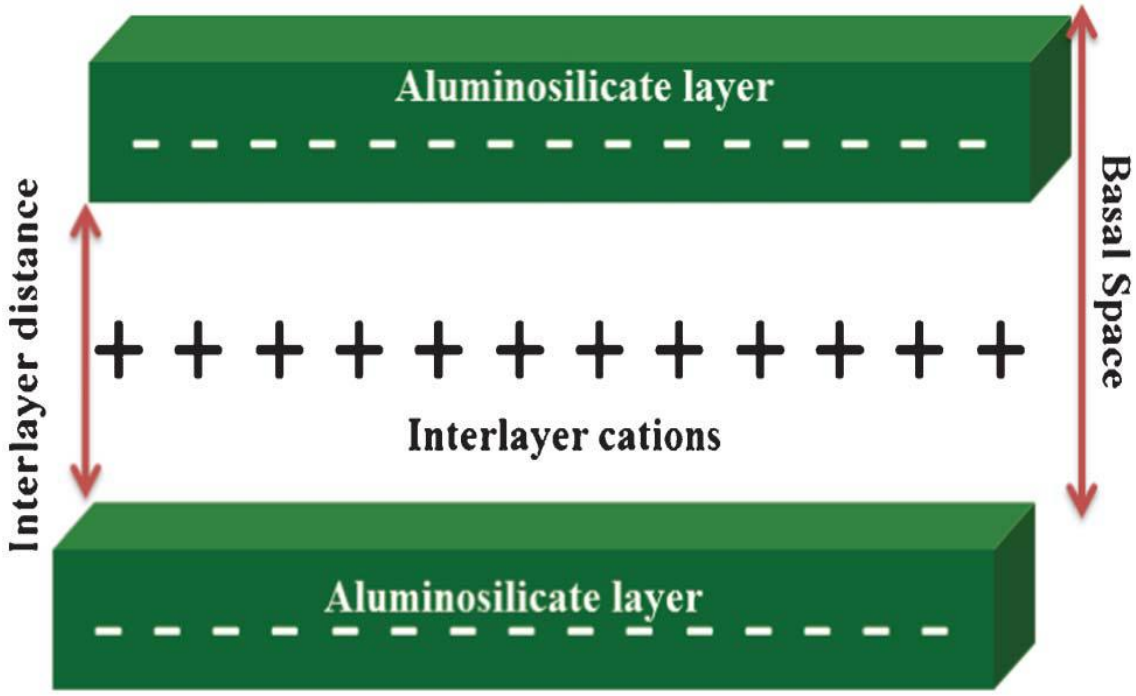

Fig.1.4: Layered structure of Clay minerals(MMT) [20].

Nanoclays are studied extensively for their use in nanoclay filled composite, surface properties, stability and for fabrication of novel compositions. Nanoclays have n beeutilized in the wide range of fields, including medicine, pharmacy, cosmetics, catalysis, food packaging, textile industry. Nanoclays are also useful and effective in environmental remediation. There is potential adsorbent for volatile organic complexes, and organic or inorganic pollutants in the soil or waste water.

Layer Type/ tetrahedral-Octahedral Sheets arrangement	**Interlayer Material**	**Group**	**Species**
1:1/T:O	None/H2O	Kaolin-Serpentine	Halloysite, Kaolinite, dicite [1, 10]
2:1/T:O:T	Exchangeable cations	Smectite, Mica, Vermiculite	Illite, montmorillonite, [1]
2:1:1/(T:O:T):O	Exchangeable cations	Chlorite	Nimite, chamosite [1, 10]

Table 1.1: Classification of clays based on arrangement of sheets

In surface modification, compatibility with the organic and inorganic medium is tried to achieve. So that better dispersion with polymeric structures or organic molecules can be achieved and can be exploited for further studies. The cations in the galleries of MMT are generally exchanged with alkylammonium/nium ions. The surface modification is carried out by replacing the alkali cations within the galleries (exchangeable cations) along with onium attached with hydrocarbon chains. several substituents of phosphonium cations (primary tertiary and quaternary) can be utilized as surfactants. The chemical structures of surfactant which is being used to modify MMT is presented in Fig. 1.5.

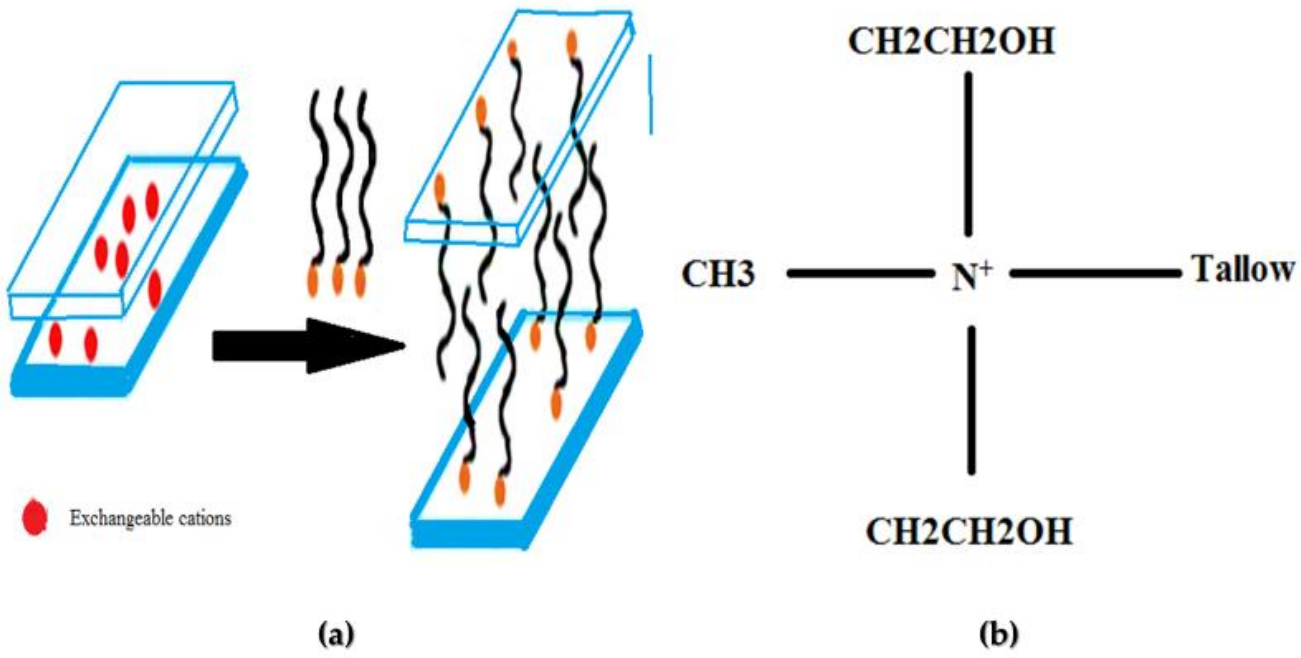

Fig. 1.5: Organophilic modification of Clay (MMT) into Cloisite 30-B [10] **(a)** and onium ion **(b)**.

The diversity in applications is due to

(1) the number of ways to modify nanoclays
(2) dispersion of layers of clay into distinct lamellae.

Amenability of these minerals for modification is due to the replacement of concerning cations or molecules within the galleries of the nanoclays by simple processes. Easy modification of the surface chemistry enables to alter the characteristics of nanoclays such as polarity, pore size, pore volume, high aspect ratio, surface area and interlayer spacing [20].

Adsorption of metals on surface of clay minerals is generally due to, H-bonding, weak van der Waals and hydrophobic forces. Employing metal oxides nanoparticles for modification of clays or clay mineral enhances the properties of nanocomposites as it has; (1) the amphoteric surface groups in nature which function as an acid / base, relying on the pH of solution;

(2) relatively large surface energy along with reaction activity due to large surface area;
(3) promising physical and chemical characteristics mainly catalytic, swelling capability, optical and electronic properties and 4) larger dispersibility of Nanoparticles and mechanical strength.

1.5. Adsorption Phenomenon:

Considering the adsorption phenomenon of toxic metal ions over surface of clay minerals, adsorption thermodynamics, equilibrium and kinetics are important parameters for effective calculation of adsorption parameters and sorption mechanism. Adsorption isotherms explain the equilibrium relationship of concentration of adsorbte in the liquid and solid phase (adsorbent surface) over uniform temperature and pH of solution. Adsorption equilibrium is reached adsorption plus desorption rates of adsorbate on adsorbent surface being equal. The models explaining such processes are usually explained graphically showing the concentration of solute in the solid phase (qe, mg g^{-1}) compared to its remaining concentration in solution phase (Ce, mg L^{-1}). The earliest and widely used model to correlate adsorption equation and experimental data was developed by Langmuir and is the most suitable model equation for explaining physical or chemical adsorption processes in liquid phases. Graphically, isotherm is explained using plateau curve, shows subsequent adsorption /desorption cannot occur after saturation. This isotherm model equation defines Henry's law behavior at low solute concentration within; on the other side, at a higher solute concentration, the adsorption saturation point will be reached. Other empirical/ semi-empirical model equations have been formulated, to explain adsorption phenomenon featuring fundamental kinetics, thermodynamics and suitable agreement for wide series of concentrations. Suc models are Langmuir–Freundlich, Hill, Temkin, Flory–Huggins, Dubinin–Radushkevich, or Sips, and Brunauer–Emmett–Teller adsorption equations.

For proper explanation of sorption behavior, the other most important factor is adsorption kinetics, it calculates the adsorption rates and pollutants desorption in a solid-solution system. The whole rate of adsorption is generally controlled by few of the succeeding steps:

(1) transport of the solute in solution (bulk solution);
(2) solute diffusion across the pseudo liquid film neighboring the solid;

(3) solute diffusion in liquid enclosed within the pores of solid and along the walls of pores (intraparticle diffusion); and

(4) adsorption/desorption of solute from the surface of solid.

In this regard, some frequently applied mathematical model equations for explaining the sorption kinetics of specific system are Elovich equations, zero-order, pseudo-first order, pseudo-second order and intraparticle diffusion. These models are associated with reaction kinetics of surface as rate-limiting step offering some advantages, mainly compactness and simplicity essential for the analysis of the rate equations.

Chapter 2

Literature Review

The utilization of clay minerals for purification of water was first investigated by Madsen and group in the end of 20th century. They had used clay to treat the turbid water, removal of particulates and microbes have been observed. Soon after this work, Churchman and his fellows studies the water remediation properties of range of clay minerals, including palygorskite, Arumpo and Wyoming bentonite, organically treated bentonite. Bentonite clay was treated with long-chain quaternary ammonim salt dimethyldtadecylamonium bromide. The results showed encouraging activity of employed group of clays [26].

The family of nanoclays were considered as promising materials because of thier outstanding properties, layered structure and suitability of dimension of their pores, stability at acidic and extreme mediums. A group of clay family kaolin was study for catalytic activities upon its physiochemical properties [27]. Clay provided the advantage of microporous structures along with high surface area, chemically nonhazardous behavior, layered structure, polarity of surface to influence the adsorption phenomenon over several microporous structures mainly naturally existing zeolites and molecular sieves. In 2010, Diatomite amorphous form of silica was exploited for combining such properties of clay minerals and enhance adsorption of a radioactive material thorium [28]. Another research group as exploited a silicate clay, palygorskite because of its property to adsorb several exchangeable cations due to isomorphic substitution, porous structure and cation exchange capability which benefited the adsorption of heavy metal cadmium from solution [29].

Abollinoa et al, in 2003 proposed a member of smectite family, Na-MMT as promising barrier in landfills for prevention of soil and ground water pollution. They reported Na-MMT a favorable adsorbent for heavy metal ions (Cd, Cr, Cu, Mn, Ni, Pb and Zn) over a range of pH, in the existence of ligands and in natural conditions [30]. Similar trend for water treatment

was reported by Kennedy et al, for Zn and Cd metal ions, they have used acid treated montmorillonite-illite clay. Acid treatment was carried out to understand the chemical stability and activity over range of pH [31].

The clay structures have ion exchange properties so their adsorption capacity can be altered by exploiting this property along with the functionalization of nanoclay structure. Modification of montmorillonite (MMT) into organoclays by grafting of molecules is carried out, these grafted molecules showed excellent properties due to presence of covalent bond of grafted molecules with clay matrix. Amine functionalized bentonite was prepared by grafting 3-aminopropyl trimethoxysilane over sodium bentonite (Bent), and for carboxylate functionalization, succinic anhydride reacted with amine functionalized bentonite. The conversion of MMT into amino and carboxylate functionality increased the adsorption of metal ions from aqueous system specifically Pb(II), Hg(II) and Cu(II) ions also proposed the material for wastewater and industrial treatment [32].

The applicability of clay family over all heavy metal ions removal, increased its utilization as water remediating agent. In 2003 Maybrook studies adsorption properties of two clays red and green for copper metal ions over a range of pH, the results supported the employment of such clays as adsorbent [33]. The functionalization or modification of clays, impart positive effects which opened a new dimension of clay utilization. Modification of clay was done either by chemically using functional groups, forming derivatives of clay minerals or using other materials and nanostructures. Susmita et al have reported the kaolinite, MMT and respective poly (oxo zirconium) and tetrabutylammonium derivatives for removal of cadmium ions. Functionalization didn't prove much effective, as functionalization with larger groups closed the pores and made them inaccessible to metal ions [34]. The activation of clay using sulfuric acid was an attempt to introduce more porosity, larger pore size, and specific surface area. the acidification of red and green clay showed better lead retention, then other adsorbent materials mainly silica and activated carbon [35]. To enhance the adsorption capacities of clay minerals, along with surface modification, intercalation of some new organic, inorganic or polymeric structure was accomplished. A similar approach was carried out by Ageetha and research fellows to remove Rh6G dye. The basic idea was to combine the improved dispersion capabilities of clay within aqueous solution and to achieve enhanced selectivity, regeneration

of nanocomposite, working at extreme conditions and mechanical strength. They have utilized organ modified montmorillonite and intercalated it with chitosan. The results exhibited that used nanocomposite is appropriate for adsorption of dyes and can be exploited for removal of toxic metal ions by further modification of organ modified clay [36]. Another attempt was carried out for detection of toxic metals ions, As (II) and Cu (II). Synthesized chitosan was intercalated in nanoclay known as heulandite [37]. The adsorption activity of metal ions was endothermic and spontaneous. Incorporation of the stabilizing agent for chitosan within the clay structure is necessary, as in most case chitosan and other intercalated molecules showed instability during adsorption process. Instead of using stabilizing agents some metal oxides and organic moieties can be grafted over clay surface to minimize the synthesis steps and better performance.

Chitosan (CTS) a naturally occurring polysaccharide materials, is suitable for sorption activity due to its larger amino contents by complexation phenomenon between amine group and heavy metal ions. Preparation of polymer clay nanocomposite has been achieved to use nanocomposite as promising sorbent for heavy metal ions and dyes. Wang and Wang used the CTS/clay (montmorillonite) as adsorbent for Congo red, the retention was higher for herbicide clopyralid from aqueous solution. The removal of humic acid and some dyes (methyleine blue, dye RR222) wastewater employing nanocomposite showed better adsorption but the preparation of nanocomposite lead to instability of structure. The CTS were usually incorporated through intercalation phenomenon within galleries of clays. These types of structures are not much stable for treatment of strong acids. Introduction of third component which is compatible to both material can help in this regard. Damai cen and fellows tried to solve this issue by incorporation of, magnetic structures into clay and then CTS supported the stability of structures. Also improved the adsorption capability and separation of nanocomposite after adsorption activity. The prepared nanocomposite was used for Cr (VI) adsorption, the removal process showed better results for CTS/MMT/Fe_3O_4 nanocomposite along with better stability upon the variation of pH [39]. Cellulose/clay composite showed effective removal of chromium from aqueous waste, the adsorption percentage was calculated to be (99.5%) using 0.5 to 0.6 g of adsorbent. Similarly, Japanese volcanic mud known as Akadama clay, modified with some salts of metals ($FeCl_3$, AlCl3, $CaCl_2$, $MgCl_2$, and $MnCl_2$) and investigated for adsorption of Cr (VI) from industrial water. The adsorption activity was

not affected by the variation of pH solution. The acid activation along with the modification of clay showed better removal, until the iron ions became insoluble in the solution. Two steps modification was reported for removal of elemental mercury, in this case clay with pillared titanium (Ti-PILC) grafted with salt of iodine potassium iodine (KI). The impregnated clay showed favorable removal of metal ions. Modification of clay K-10 with the ammonium pyrrolidinedithiocarbamate (APDC) showed better adsorption for cadmium and manganese the unmodified naturally occurring K-10. On the other side grafting of red clay with hexadecyltrimethylammonium bromide (HDTMA) showed excellent adsorption capacity for chromium Cr(IV) [41].

Palygorskite (Pal) and sepiolite (Sep) the fibrous clays having 2:1 ribbons like structure, which are laterally linked due to basal oxygens. This type of structural arrangement leads to larger surface area plus better desorption activity for organic compounds. Modification of such clay minerals with organo-alkoxides having groups, like amine, mercapto/chlorine, improved remediation process for various pollutants. The functionalization of clays with alkoxide 3-aminopropytrietoxysilane (APTES), showed higher removal of Metanil yellow (MY) and Methylene blue (MB). Chemical grafting of clays with aminosilanes showed better adsorptive capacity [42]. Iron oxide nanoparticles incorporated on the surface of clay(K-10) was reported as a catalyst for improved Friedel–Crafts benzylation reaction employing benzyl alcohol and benzyl chloride [43].

Sepiolite a magnesium silicate having repetition of tunnels and blocks arranged in fiber. In the rectangular fibrous structure cations are mainly Ca and Mg. The clay showed the capacity of uptake of dyes (methylene blue (MB) / violet dyes), the uptake is due to the cation exchange property and neutral sites. Subsequent processes such as saturation of sodium/calcium for enhancement of adsorption capacity is also reported. Modification using quaternary amine (hexadecytrimethylammonium bromide, HTAB) provided proper adsorption of dyes. sepiolite clay mineral for textile azo dyes was also studied and sepiolite proved as decent adsorbent for removal of azo dyes [44]. Modifications of clay mineral (bentonite) with prepared magnesium ferrite nanoparticles (MgFe2O4 NPs) was carried out for wastewater treatment. Bentonite, have significant content of montmorillonite in its structure. The proposed material was blend of high surface area and char properties of bentonite and easily separable magnetic, and

adsorptive attributes of nanoparticles. The prepared blend had promising adsorptive, magnetic characteristics and consequently regeneration after adsorptive activities. The uptake of chromium metal from aqueous waste proved the used material as reusable, economically viable and effective hybrid adsorbent [45].

Sorption of copper metal on Na+ cloisite (a member of smectite family of aluminosilicates) was studied. The adsorption is basically due to the surface reactions and metal binding on adsorption sites. The adsorption of metal ions at low pH because of formation of outward sphere like surface covers the cared basal sites at surface, at higher pH because of varying sites at surface due to formation of inner sphere like surface [46].

Modification of clays minerals mainly montmorillonite by embedding organic materials and function groups (organic derivatives of ammonium) having various chelating functionalities, not only favorable for removal of heavy metal ions, have favorable characteristics for biodegradable coating as well. Recently, organically modified Na+-cloisite with organic ammonium salt for preparation of bionanocomposite. The organomodified clay was dispersed in the polymer polyvinyl alcohol (PVA) through hydrogen bonding plus hydrophobic interactions. The incorporation of organomodified clay, enhanced the thermal stability and char, resulted in the preparation of bionanocomposite [47]. For industrial waste treatment MMT modified with organometallic structures, named as Cloisite 30B was investigated. The purpose is to use the amphiphilic nature of clay with the care surface of naturally occurring polymer chitosan. The prepared nanocomposite worked as promising adsorbent materials for dyes (RB-21 and RR-141). In this method, the dyes were adsorbed over the surface of clay matrix rather to intercalate in the galleries. The adsorption capacity was found to be maximum for dyes then previously reported adsorbents. The higher adsorption capacity is due to the collective adsorption by chitosan trough hydroxyl and amino groups and amphiphillic surfactant (organoclay) along with functional group (ammonium having alkyl chains and the other ones are hydroxyl groups) also higher zeta potential at lower pH. All such properties enhanced removal of dyes [48]. The amphiphilic nature of organomodified clay, its mechanical strength and stability at elevated conditions have attracted the attention of researchers to exploit it not only for mechanical properties but also for other applications. Recently Cloisite 30-B is used as a compatibilizer and reinforcing agent, to enhance the

mechanical strength and stability of prepared nanocomposite. The nanocomposite has matrix of polymers Polyimide (PI) and Polysulfone (PSF) with the filler Cloisite 30-B. Incorporation of nanoclay for inducing compatibilizer effects also prompted significant reduction with in aspect ratio of phase distinguished domains at surface of film. This effect of compatibilizer over phase separation can be exploited in sensing. The prepared blend film was used as oxygen barrier because of addition of Cloisite 30-B clay in blend film. The addition of organoclay successfully increased the viscosity of film [49].

Hybrid of inorganic chitosan and MMT modified organoclay namely (Cloisite 10A) for development of economical and promising adsorbent for heavy metal ions was synthesized. The incorporation of organoclay support in the adsorption phenomenon and reusability. This hybrid was prepared to combine hydrophilic property of inorganic polycation along with retention of inorganic polyanion. The hybrid enabled the adsorption studies over wide range of pH [50].

The carried research showed the favorable attributes of organoclays as adsorbent of heavy metals, for higher adsorption the modification of such clays with materials showed improved adsorption activities. For this, nanostructure mainly nanoparticles, Nano spheres, coatings or films can be grafted or adsorbed over the surface. To achieve such characteristics Luiz et al, adsorbed iron oxide nanoparticles over the surface of nanoclays, the adsorption of enables higher surface area and provides proper support to nanoparticles. In this case agglomeration of nanoparticles can be avoided. The adsorption activity is due to both nanoparticles and clay, along with enhanced activity for adsorption they facilitated the separation of composite. Iron oxide nanoparticles ad larger content of phase maghemite ($g\text{-}Fe_2O_3$), which was further proved by other characterization tools [51].

Coating of MnO_2 on montmorillonite k-10 was achieved to investigate the electrochemical properties of prepared nanocomposite. The prepared nanocomposite has improved micro or nanotextural properties, which comprises surface area, pore distribution, pore dimension, volume and distribution. Porosity and surface area favored the chemical properties of composite. These electrochemical properties can be exploited for the sorption of hazardous

metal ions as both components of matrix affinity towards metal adsorption [52,53]. Similarly, grafting of montmorillonite clay with iron oxide nanoparticle for removal of chromium metal ion, was accomplished. In this case decoration of nanoparticles over montmorillonite was carried out in two ways, to optimize the route for synthesis of nanocomposite as adsorbent. The physical mixing of Fe_3O_4 nanoparticles showed better performance as in this case the narrow distribution of nanoparticle size was achieved, in case of in situ attachment of nanoparticles showed agglomerates of nanoparticles and improper dispersion hence reduced adsorption activity. The adsorbent showed better stability in case of storage for long time and reusability than other nanocomposite, adsorption kinetics favored its use as adsorbent for water treatment. In this analysis, pure Fe_3O_4 nanoparticles were also used for chromium removal but the removal was not satisfactory. This is due to the agglomeration of nanoparticles with in the solution and reduction of surface area which is primary for metal bonding [54].

Surface decoration of clay minerals with iron oxide magnetic nanoparticles have defined a class of composite materials as adsorbents of both inorganic/organic pollutants. Magnetic nanocomposite can be easily separated from solution after adsorption activity. Such nanocomposites have adsorption due to amphoteric behavior of magnetic nanoparticles and ion exchange or physical interaction by clay matrix. For adsorption, different phases of iron oxide can be used at the same time can be used for adsorption studies. Adsorption phenomenon of nanocomposite was spontaneous having better stability of adsorbed ion over the surface [55]. The magnetic magnetite nanoparticles had better adsorption capacity towards most of the hazardous heavy metal ions. Such wide applicability of Fe_3O_4 nanoparticles make them effective to use as adsorbent. For excellent adsorption, they must be used with the support, to maximize their surface area and avoid agglomeration [56].

Manganese oxide nanostructures, have attracted growing importance due to unique fundamental characteristics and their wide applications in several fields such as catalysis, sensing, magnetism, energy storage and converting devices like supercapacitors, and lithium ion batteries. Due to economical raw materials, variation in structures, minimum toxicity, also environmentally friendly properties they are frequently exploited in various fields. Amongst

all the crystallographic structures of manganese oxides, tunnel structure is getting substantial attention because of its thermodynamic stability and larger catalytic activity, particularly for the 2 x 2 tunneled structure. This material has been employed as catalysts using benzyl alcohol oxidation to benzaldehyde, in case of catalytic behavior, amount of active oxygen at lattice sites, acidic sites, surface area, crystallinity, size of particle along with crystal structure affected the catalytic performance. The acid sites and active lattice sites have provided more opportunity for adsorption [57]. Same kind of study using MnO_2 was carried out by Mohammad and his fellows, they have successfully prepared the structures having manganese oxide synthesized on different metal oxides and porous structures. The chemical activity of manganese oxide supported the water oxidation catalysis and production of hydrogen which further utilized for transformation of intermittent energies [58].

Recently few attempts were performed to use both MnO_2 and magnetic iron oxide nanoparticles for the removal of heavy metal ions. The study revealed that incorporation of MnO_2 nanoparticles and Fe_3O_4 nanoparticles in the matrix, exhibited excellent removal activity. Along with metal retention, they had better reusability and easy magnetic separation ability. The stability, adsorption capacity and removal kinetics of nanocomposite comprising such nanoparticles can be enhanced by varying supporting material or matrix, loading content of nanoparticles and their crystallographic structure [59].

Chapter 3

Materials and Methods

3.1. Materials:

$Fe(SO_4)_2.7H_2O$, $FeCl_3.6H_2O$, $MnSO_4.H_2O$, $KMnO_4$, H_2SO_4 and $NH_4.OH$ were purchased from Sigma Aldrich and utilized for the synthesis of Nanoparticles. $Fe(SO_4)_2.7H_2O$, $FeCl_3.6H_2O$ and $NH_3.OH$ are used for the synthesis of Fe_3O_4 nanoparticles while MnO_2 nanoparticles were synthesized by utilizing $MnSO_4.H_2O$, $KMnO_4$ and H_2SO_4. For the preparation of nanocomposites Cloisite 30-B (southern clay products) was used. DI and distilled water are used as a solvent in chemical reactions.1,5-diphenylycabazide, acetone, H_3PO_4, HCl (Merck) and NaOH (Sigma Aldrich) are used for calorimetric detection of chromium ions. All the chemicals didn't require any purification steps prior to use and of analytical grade.

3.2. Synthesis of nanoparticles:

3.2.1. Synthesis of iron oxide nanoparticles:

Iron oxide nanoparticles were synthesized by using Co-precipitation process. The molar ratio of precursors, $FeCl_3.6H_2O$ (6.1g) and $Fe_2SO_4.7H_2O$ (4.2) was taken as 2:1 for the synthesis of nanoparticles. At first, FeCl3.6H2O was added into a beaker containing 100ml distilled water and a magnetic stirrer, subsequently, $FeSO_4.7H_2O$ (6.1g) was added into the solution under stirring and nitrogen gas was purged into suspension till the completion of the reaction. The clear suspension of both salts solution was prepared by stirring at 700rpm for 10 mins; the stirring rate was kept constant during the whole reaction. The temperature of the suspension was raised to

90 ^{o}C. At 90 ^{o}C 10 ml NH_4OH was added rapidly in the solution to neutralize it. Addition of base/reducing agent initiated the nucleation and growth of nanoparticles. The reaction was carried out for 30 min at 90 ^{o}C with continuous stirring under inert conditions. Soon after the addition of ammonium hydroxide the pH was between 10-12. After the end of the reaction, the product was kept for few hours to settle down the precipitates. For the removal of ions (chlorides and sulfates etc.), the product was washed using DI water. For washing, the product was transferred into falcon tubes and centrifuged at 4000rpm for 30mins. The supernatant was removed, water was added into tubes followed by sonication for 10-15 min. Sonication was carried out for gentle mixing of precipitates in water and hence complete removal of ions and impurities. This process was carried out for six times and after complete washing the pH was about 7. The precipitates were removed from falcon tubes and collected in a beaker and dried at 80 ^{o} C in vacum for 14 hrs. The dried product was crushed in mortar pestle to obtain the fine powder of Fe_3O_4 nanoparticles. Figure 3.1. shows the schematic representation of synthesis of nanoparticles using co-precipitation [60].

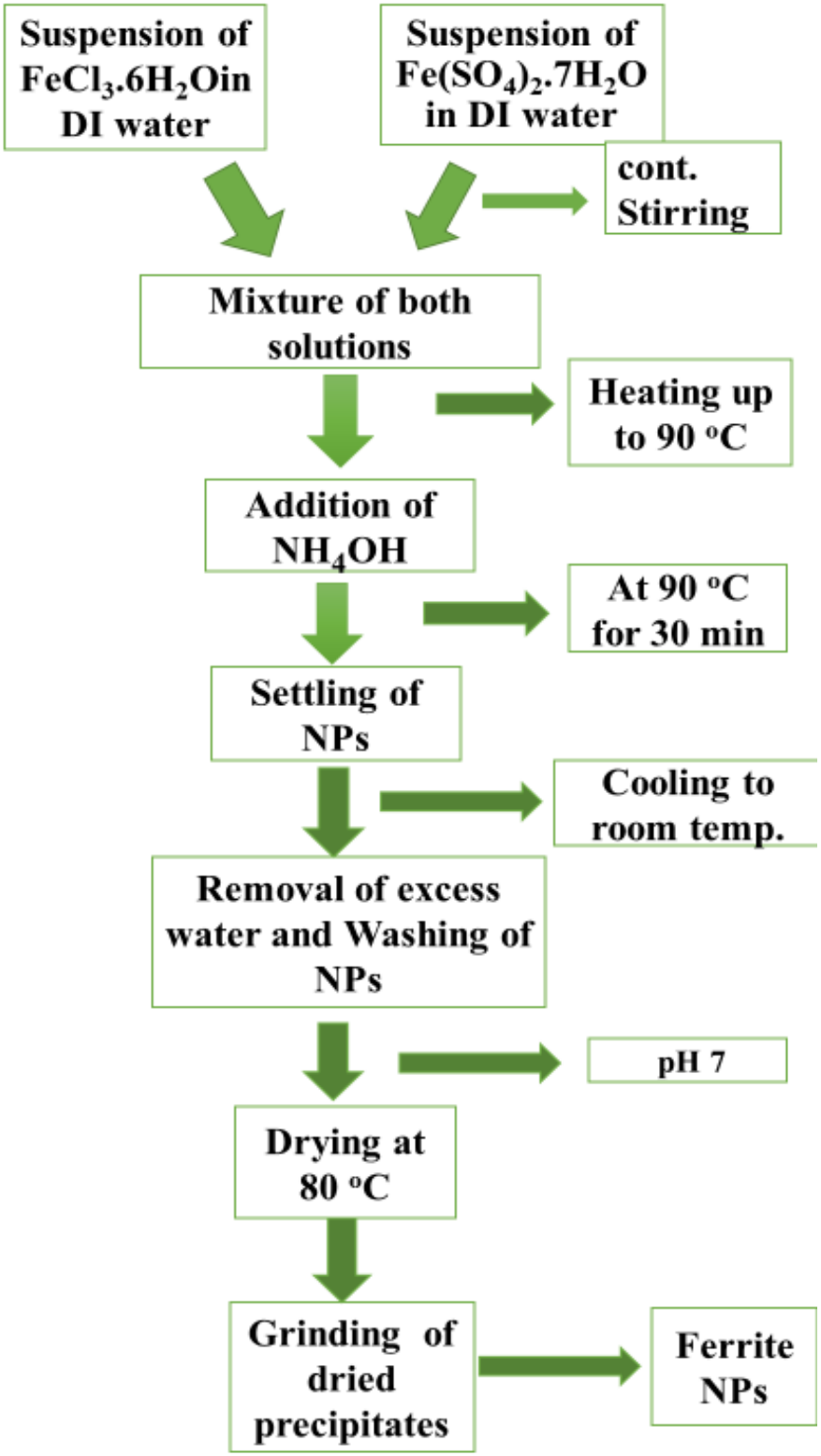

Fig.3.1: Flow chart for the synthesis of iron oxide NPs.

3.2.2. Synthesis of manganese oxide nanoparticles:

MnO_2 nanoparticles were also synthesized using co-precipitation route [61]. Metal salts such as $KMnO_4$ (3.9g) and $MnSO_4$. H_2O (8.45 g) were used in the molar ratio 0.5:1. Both precursors were added separately in a beaker having 50ml dist. water and magnetic stirrer, placed on a hot plate for 15 min with stirring to obtain a clear solution. The solution of $KMnO_4$ was transferred to three-necked round bottom flask in an oil bath. Subsequently, the solution of another precursor ($MnSO_4$. H_2O) was put into the flask under continuous stirring. The stirring rate was kept constant throughout the reaction and temperature of solution was raised to 70 ^oC and heating continued for 4hrs. After completion of reaction, the product was placed overnight to reduce the temperature of solution down to room temperature and settling of precipitates. The removal of ions and impurities was done by washing where pH of the solution was raised from 1 to 6. The solution was poured into falcon tubes and centrifuged at 4000 rpm for 15 min. The washing process of MnO_2 nanoparticle was carried out by centrifuging the solution. The supernatant was discarded subsequently distilled water was added. Washing was carried out 7 times followed by final washing with ethanol. Afterward, the precipitates were transferred into a beaker from tubes and dried at 110 ^oC for 5 hrs. in a vacuum oven. The dried product was grounded in an agate mortar pestle to obtain a fine powder. The fine powdered was placed in a china dish and calcined at 300 ^oC for the removal of any moisture and proper formation of crystalline phases of nanoparticles. After calcination, the powder was again grounded to obtain fine powder without any larger grains.

Acidification of powder was also carried out in a three-necked round bottom flask placed in an oil bath. For acidification, 100ml of 2M solution of H_2SO_4 was used and 3g of dried powder was added into the solution of sulfuric acid. The solution was heated to 90 ^oC and kept at that temperature for 2 hrs. The solution was kept for few hrs. to lower the temperature followed by washing of precipitates using distilled water. Solution was centrifuged, the supernatant was discarded followed by sonication by adding water. These steps were repeated 8 times to make the precipitates pH neutral. Precipitates were dried at 100 ^oC for 9hrs and finally, dried product was grounded into fine powder of MnO_2 nanoparticles. Fig. 3.2 shows the steps of synthesis of MnO_2 nanoparticles.

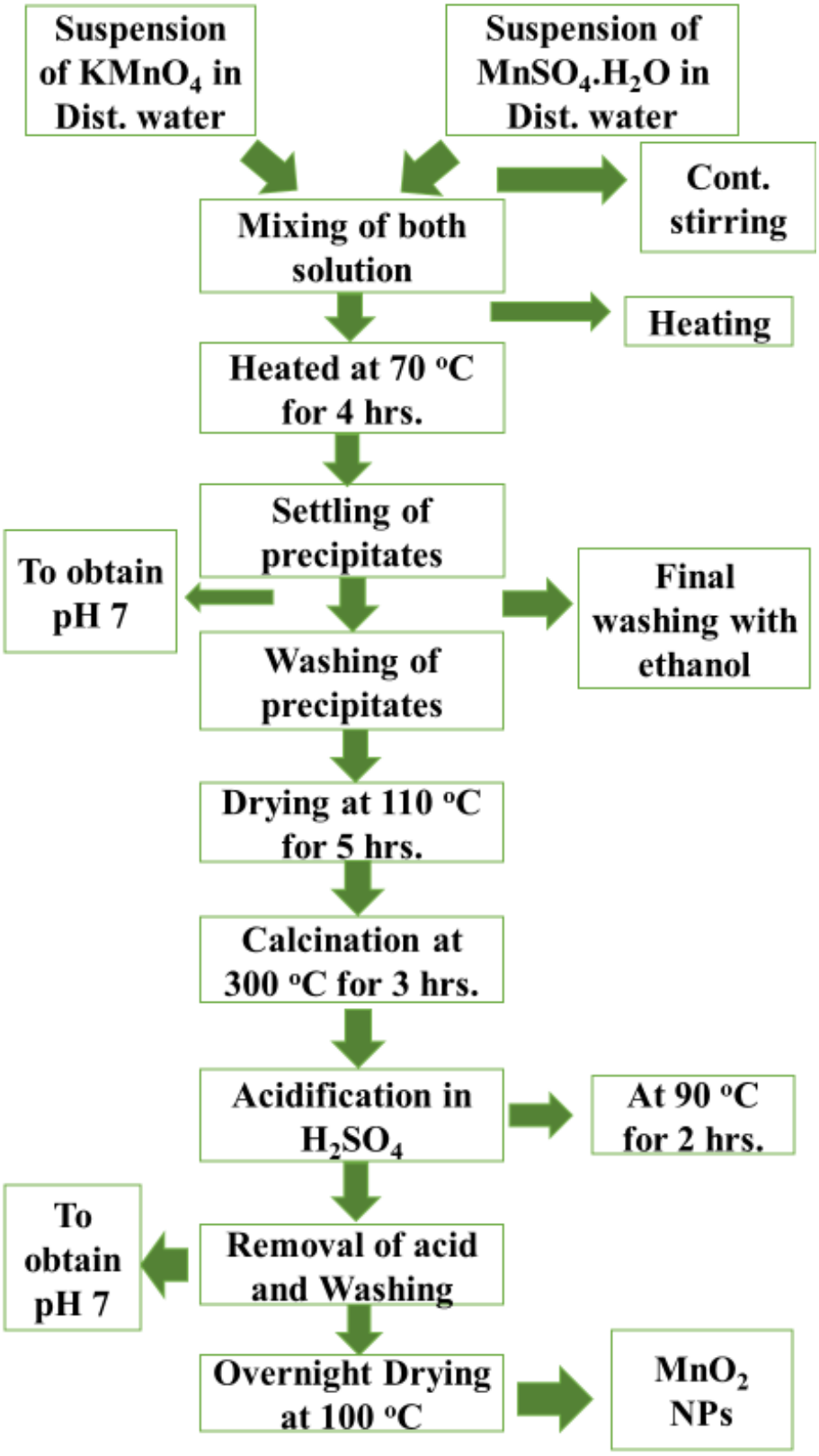

Fig. 3.2: Synthesis of MnO_2 NPs

3.3. Synthesis of Nanocomposites:

Composite of MnO_2, Fe_3O_4 and clay was synthesized in two steps. In first step nanocomposite of Fe_3O_4 and clay was prepared [61]. Secondly MnO_2 nanoparticles were adsorbed on clay/Fe_3O_4 nanocomposite, adsorption of MnO_2 nanoparticles was done by ultra-sonication and physical route was adapted [62].

3.3.1. Synthesis of Fe_3O_4/Clay nanocomposite:

For the synthesis of Fe_3O_4 and clay nanocomposite, hydrosol of Fe_3O_4 nanoparticle was prepared. Hydrosol was prepared by the reported method [61]. At first, Fe_3O_4 nanoparticles were synthesized. Nanoparticles synthesis protocol was same as mentioned above with only difference in the use of nanoparticles without drying. After washing the precipitates were added into 50ml of 0.01M HCl under continuous stirring. The addition of acid is to neutralize the charge of nanoparticles. After stirring for 15 min the suspension was transferred into falcon tubes and centrifuged at 4000rpm for 5 mins. The precipitates were separated and supernatant was discarded, the nanoparticles were peptized by adding DI water. Water was added untill the pH of solution reached to 4. The solution was placed for 3hrs for settling down the solids and black colored supernatant was collected. After preparation of hydrosol, the suspension clay was prepared by adding 0.5g of clay in 10ml DI water and stirred for 10 mins.

Later, equal volume of hydrosol to clay suspension was added into clay suspension and stirred for 30 mins. After sufficient stirring solution was then centrifuged at 4000rpm for 5 min, clear transparent supernatant was removed, 10ml of hydrosol was added and again centrifuged at same conditions. This process was repeated 9 times where in last step the supernatant was not removed but the solution was used for the synthesis of Fe_3O4/MnO_2/Clay nanocomposite. Figure 3.3 shows the flow chart for the synthesis of Fe_3O_4/Clay nanocomposite.

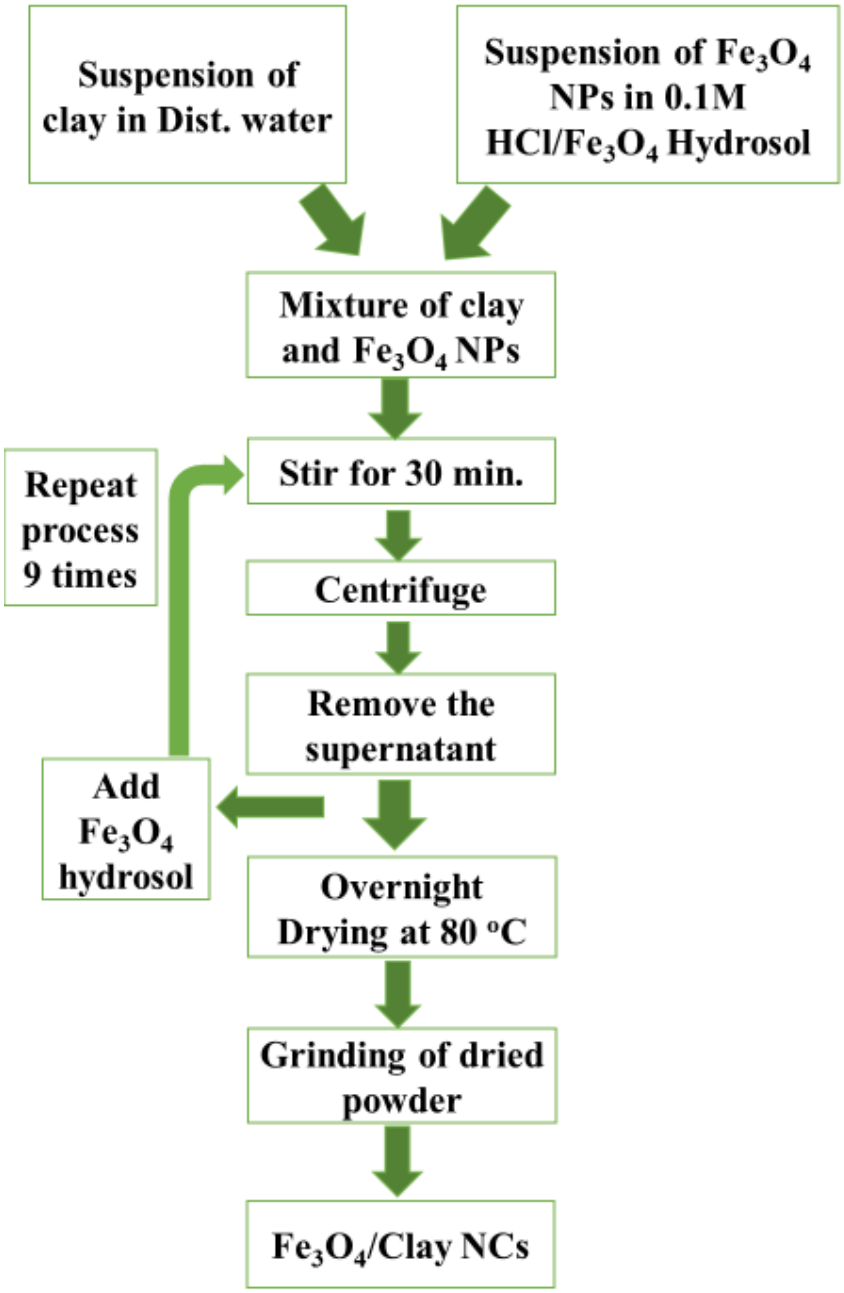

Fig.3.3. Synthesis of Fe_3O_4/Clay Nanocomposite

3.3.2. Synthesis of Fe_3O_4/MnO_2/Clay nanocomposite:

Nanocomposite of Fe_3O_4/MnO_2/Clay was prepared by using 5 wt./vol.% of MnO_2 nanoparticles and 10 ml solution of Fe_3O_4/clay nanocomposite. For 5 wt./vol.% of MnO_2, 0.35g was added into 7ml DI water then sonicated for 30 minutes using probe sonicator to achieve homogeneous dispersion of nanoparticles. After sonication of nanoparticles, the stirred (30 min) suspension of Fe_3O_4/clay was added in to the solution of 5wt. /vol.% of MnO_2 and sonicated for 2 hrs. The solution was dried at 80 ^oC in vacum for overnight. The dried product was grounded using mortar pestle into fine powder and kept in air tight glass vial. Figure 3.4 shows the steps of the synthesis of Fe_3O_4/MnO_2/Clay nanocomposite.

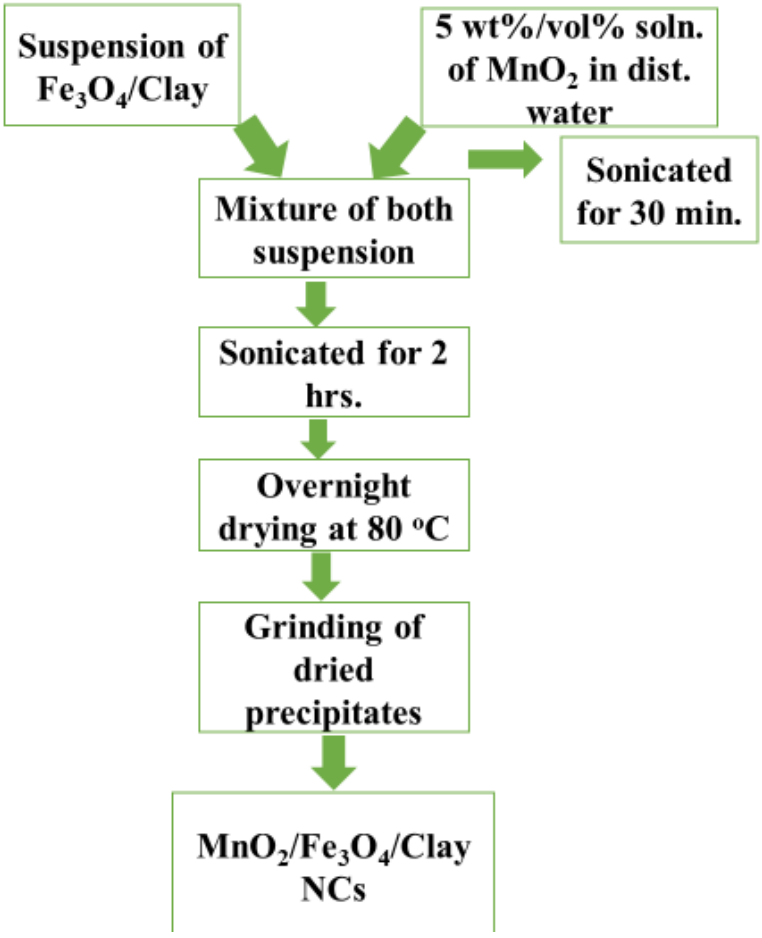

Fig.3.4: Flow chart for the Synthesis of MnO_2/Fe_3O_4/Clay Nanocomposite.

3.4. Characterization of nanoparticles and nanocomposites:

The following characterization tools have been employed for analysis of synthesized Fe_3O_4, MnO_2 nanoparticles, nanoclay, FE_3O_4/Clay and MnO_2/Fe_3O_4/Clay nanocomposite.

a) X-ray diffraction for crystallographic structure
b) Scanning electron microscope for analysis of surface morphology
c) Fourier transformation infrared spectroscopy
d) UV-Vis spectrophotometer (PG Instrument T90)

3.4.1. Scanning Electron Microscopy (SEM):

Scanning electron microscopy is technique used for analysis for imaging material's surface. Chemical composition and phase mapping of analyzing materials can also be obtain from SEM. The interactions of beam and matter resulting signals are generated which are collected and further displayed on CRT. The pattern on the screen shows the features of the sample. Generally, these interactions generate transmitted electrons, secondary and backscattered electrons, X-rays and cathodoluminiscence [63]. The beam of electron is made to raster over the surface of materials and focus on very narrow area. The surface of material will emanate electrons and photons upon interaction of beam with the sample, detectors are used to collect ejected photons or electrons. The intensity and path of beam and brightness of cathode ray tube is adjusted with the electromagnetic lenses and outputs of detectors. Hence image is achieved on cathode ray tube. Images are generated because of characteristic x-rays, back scattered and secondary electrons.

Small quantity of sample is enough for analysis. In SEM, both conducting and nonconducting samples are characterized but in case of nonconducting samples, coating of conducting metals mainly of gold is done. Otherwise accumulation of charge over the surface alters the main process. Coating

must be uniformed to avoid errors due to agglomeration of coated material. High beam voltage is used for analysis [64].

3.4.2. X-Ray Diffraction:

It is an important characterization technique for the identification of crystallinity, content of crystallinity and structure properties of a materials. Through XRD data structural strain, defects within crystal, crystallite size, phase composition and crystallographic orientation can be calculated. Atomic stoichiometry of both amorphous and crystalline powdered or thin films can be evaluated through this technique. The positions and relative intensities of peaks allow the identification of single and mixture of crystalline phase which are identical. Some chemical phenomenon's mainly phase transitions, solid-state reactions and lattice vacancies can also be calculated using sophisticated instrumentation.

It's a non-destructive technique, but sensitive to high Z-elements because of their relatively high intensities diffracted beams. For obtain diffraction patterns, methods are defined i.e. powder diffraction, rotating crystal and Laue diffraction method. Most frequently, powder diffraction method is used. Single-crystal x-ray diffraction, neutron diffraction, single crystal neutron diffraction, electron diffraction LEED and RHEED are some alternated structural characterization techniques. LEED and RHEED are useful for evaluation of information regarding surface of material. Single crystal technique resolves more complexed solution structure, neutron diffraction is sensitive to magnetic materials and require larger samples, single crystal neutron diffraction is highly sensitive to light elements and electron diffraction provides lattice information but these techniques requires highly sophisticated equipment's and environment [63].

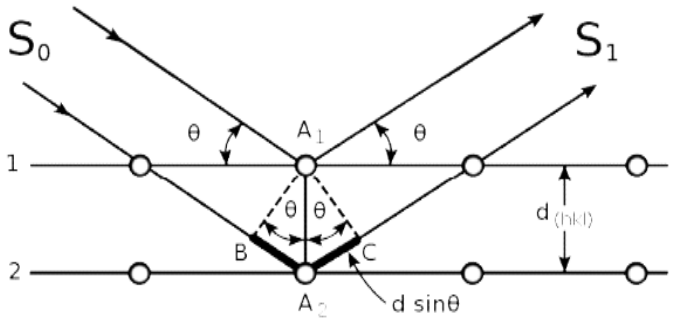

Fig.3.5: Scattering of beam by atomic planes [63].

X-ray beam is made to impinge over sample and reflected from crystal planes. The crystal planes reflect the rays in all direction that are fall on material. The periodic arrangement of planes leads to superposition of rays and only in phase rays will reach to detector. The expression explains this is known as Bragg's Law, given by

$$n\lambda = 2d\sin\theta$$

n is order of in phase interference,
θ is incident angle,
d is Interlayer spacing and
λ is wavelength of incident X-ray.

The inter planner distance (d), lattice constant, and crystallite size for XRD data can be calculated by using values of λ and θ. For calculation of lattice parameter,

$a = \lambda (h^2+k^2+l^2)^{1/2}/2\sin\theta$

and crystallite size $t = 0.9\ \lambda/\beta\ \cos\theta$

these expressions are used whereas h, k, l are miller indices of planes and β is full width half maximum respectively [65].

3.4.3. Ultraviolet/Visible Spectroscopy (UV/Vis):

Ultraviolet / visible (UV-Vis) spectroscopy also known as UV-Vis absorption spectrometry and UV-Vis spectrometry, working in the range of 190- 900nm. This is basically the relative measurement of actuated beam after reflection from the sample. Optical properties, electronic delocalization, electronic structure, oxidation states, concentration of material (reactants/ products during reaction) with in sample, metal ligand interaction and formation of new materials can be analyzed using this tool. UV/Vis origins transition with in electronic energy levels, and so can pronounced as electronic spectroscopy [66].

Higher energy Ultraviolet/visible photons cause excitation of molecules to excited state from their round state by absorbing some of photons' energy. The wavelength of emitted radiation relies on difference between round state energy and excited state generally one photon upon absorption produces excitation of one electron. This is mainly because of absorption of specific wavelength by molecules. absorption principle states that position of molecule is remain same [67].

According to Frank Condon principle, we ave four types of electronic transitions after UV/Vis absorption

1) $\sigma \rightarrow \sigma^*$ (saturated hydrocarbons)
2) $n \rightarrow \sigma^*$ (hetero-atoms)
3) $\pi \rightarrow \pi^*$ (conjugated systems)
4) $n \rightarrow \pi^*$ (hetero-atoms having conjugated system)

The absorption intensity is directly related with the amount of materials and their position. At specific wavelength intensity relates with the number of molecules absorb the energy of that specific wavelength. The expression for absorption intensity is expressed as

Where,
I_0 = incident radiation intensity
I = transmitted radiation intensity

In Case of UV/Vis spectroscopy beer-lambert law is most significant and must be followed. Law is related to absorbance, concentration and path length traveled by UV/Vis radiation

$$A=€cl$$

Where,

A = wavelength absorbance.

€= absorption intensity or molar absorptivity (L/mol cm), at specific wavelength, it is constant for solute. It calculates amount of absorbed light by the solute at specific wavelength.

c = concentration of the sample in (Mol/L) solution.

l = path length of the sample solution (cm).

For absorbance greater than 1, Beer's law doesn't hold since molecules are very close to each other and influence the absorptive properties [63].

3.4.4. Fourier transform infrared spectroscopy:

The absorption, chemical purity, presence of elements, bond type and photoconductivity of the material can be evaluated using this analytical technique. It works on infrared spectroscopy and mathematical tool Fourier transformation and hence known as Fourier transform infrared spectroscopy (FTIR). It quantifies the absorbed light over a wavelength and the presence of several groups on materials absorb hence identified. FTIR, a single beam probe, resolves all problems linked with dispersive tools.

In FTIR, a beam of infrared region falls on beam splitter, one of the splitted light beam refracted towards fixed mirror while other is transmitted through moving mirror. This transmitted light passes through sample and provides information about sample [68]. Liquid chromatography fraction, analysis of tiny samples can be analyzed using FTIR.

A Fourier transform infrared continuum was obtained in transmittance mode using Perkin Elmer FTIR spectrometer. Samples were dispersed, hydraulic pressed along with KBr powder in a pellet structure and usually Michelson interferometer is used in FTIR spectroscopy [69].

Chapter 4

Results and Discussion

4.1. Scanning Electron Microscopy (SEM)

The samples were prepared by diluting DI water based suspensions of Clay, Fe_3O_4, MnO_2 nanoparticles, Fe_3O_4/clay and Fe_3O_4/MnO_2/Clay nanocomposites. The dilutions were then sonicated for 3 hours. A drop of each sample was dropped on a piece of glass slide and air dried, subsequently coated with thin layer of gold using (JEOL JFC-1500) ion sputter to avoid accumulation of charge

Scanning Electron Microscopy (SEM) was performed on JEOL JSM 6490 (LA) at an acceleration voltage of 20 kV.

4.1.1. SEM of nanoparticles:

Images of Fe_3O_4 nanoparticles, obtained from Scanning Electron Microscopy (SEM) are shown in Figure 4.1 at different magnifications, while Fig. 4.2 shows the SEM images of MnO_2 nanoparticles. SEM reveals the prepared nanoparticles are uniformly dispersed and clearly distinguishable having narrow size distribution ranging from 16-20 nm. For MnO_2 NPs the size ranges within 14-20 nm. Nanoparticles have less agglomeration and properly separated from each other. The calculate average size of Fe_3O_4 nanoparticle was found to be 18 nm and 17nm of MnO_2 nanoparticles.

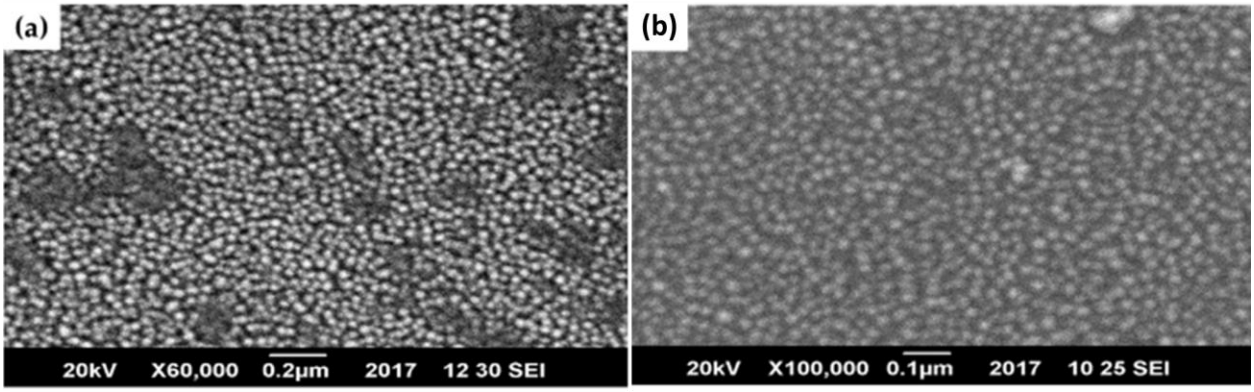

Fig. 4.1 SEM images of iron oxide NPs **(a)** and manganese oxide NPs **(b)**.

The morphology of nanoclay is shown in the Figure 4.2 (a). The surface of nanoclay free was found to be from cracks and pores and didn't have any aggregation or adsorbed species over the surface thus providing favorable conditions for adsorption of nanoparticles.

4.1.2. SEM of nanocomposites:

The morphology of Fe_3O_4/Clay shows that nanoclay is successfully covered with spherical iron oxide nanoparticles. The nanoparticles are homogeneously dispersed, without formation of aggregates. The least aggregation of nanoparticles is supporting the fact that the nanoclay provided sufficient and uniform surface for NPs to arrange themselves at minimum energy configuration. As shown in the Fig. 4.3 the size of assembled nanoparticles is between 18-22 nm this is in correspondence with that calculated size of pure iron oxide nanoparticles.

According to SEM images of MnO_2/Fe_3O_4/Clay, the loaded MnO_2 nanoparticles are properly dispersed to minimize agglomeration. These nanoparticles are loaded along with Fe_3O_4 NPs. The size of nanoparticles in MnO_2/Fe_3O_4/Clay nanocomposite is calculated as 18 nm, the nanoparticles are less agglomerated and evenly distributed. This shows that the nanoclay act as

favorable support for the adsorption of nanoparticles allowing homogeneous dispersion over the surface [68].

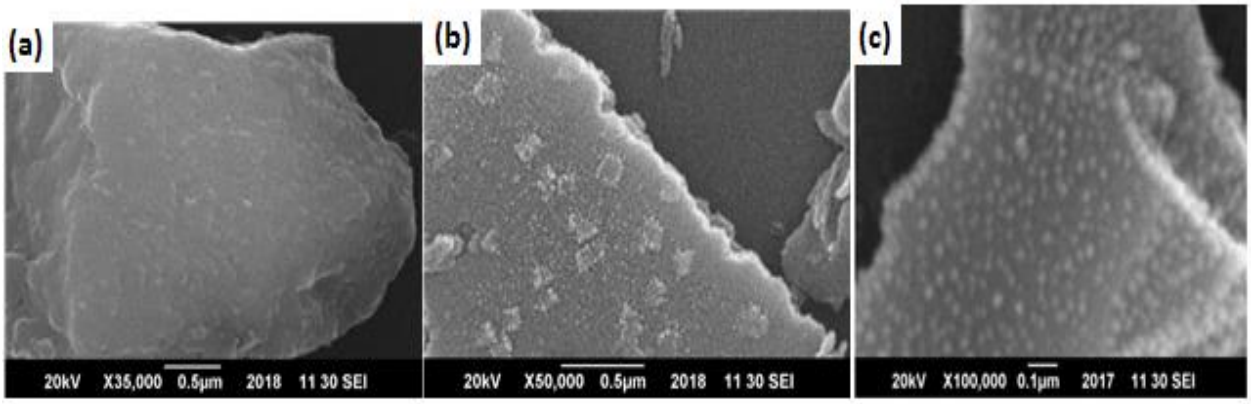

Fig.4.2 SEM micrographs of pure nanoclay **(a)**, Fe_3O_4/Clay **(b)** and MnO_2/Fe_3O_4/Clay NCs**(c)**.

4. 2. X-Ray Diffraction (XRD)

For X-Ray Diffraction (XRD) analysis, dry powders of clay, nanoparticles, and nanocomposite were used. STOE Powder X-rays Diffractometer was used for analyzing XRD results, with Cu Kα radiation (λ = 0.154 nm) from 20° to 80° (2θ). All XRD patterns are obtained at room temperature.

4.2.1. XRD data of nanoparticles:

The properly distinguishable diffraction peaks of MnO_2 nanoparticles supporting two co existing phases, orthorhombic and tetragonal [57]. Peaks at position of 2θ = 60, 49, 28, match with (160), (411), (310) referring α-MnO_2 phase and peaks at 2θ = 66, 56, 43 and 38 with crystal lattice (521), (160), (300) supporting orthorhombic phase of MnO_2 structure, this whole diffraction pattern identified as tetragonal and orthorhombic crystal structure of MnO_2 nanoparticles. The

diffraction peak intensities are showing crystalline nature of nanoparticles. The peaks at the position of 29.1, 35.2, 42.8, 53.1, 56.6 and 62.1 corresponding to the planes (220), (311), (400), (422), (511), and (440). The peaks are consistent with standard XRD pattern of spinel phase magnetite nanoparticles, as shown in the Figure 4.3 (a).

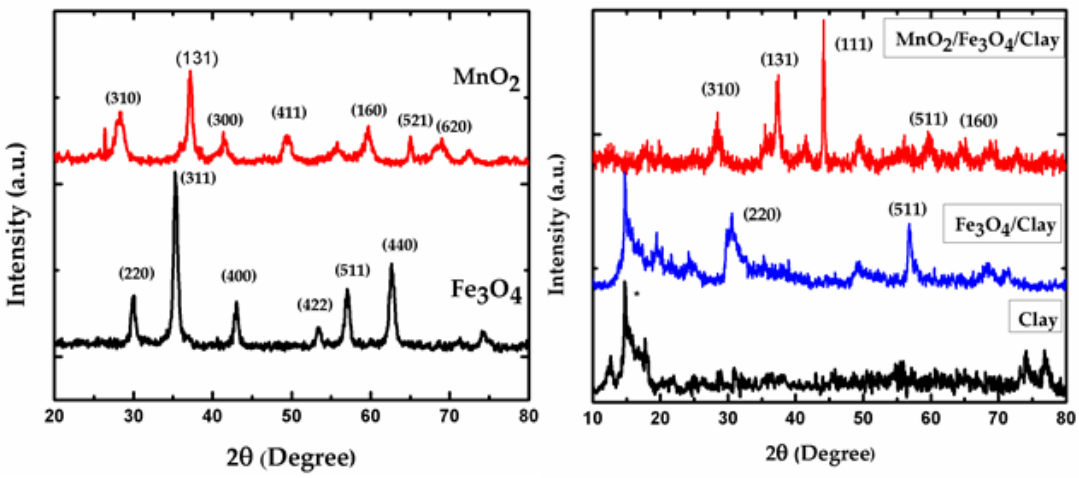

Fig. 4.3: XRD results of NPs **(a)** and NCs **(b).**

4.2.2. XRD of nanocomposites:

The structure of nanoclay is shown in the Fig. 4.5 (b). The major indexed phase is of MMT with the cloisite 30-B. The diffraction peak at position 2θ = 19.74 is due to the MMT (as nanoclay has MMT and quaternary ammonium salt within the galleries of MMT). The noise and humps in the pattern attributing the amorphous content of nanoclay [69].

In the case of Fe_3O_4/Clay nanocomposite the diffraction peak at 2θ = 19.74 is appeared while other peaks are due to the (220) and (511) planes of magnetite. Some peaks of magnetite structure have overlapped or disappeared due to noise amorphous content of nanoclay while appeared peaks have less intensity. The appeared peaks of iron oxide nanoparticles confirmed the successful loading of nanoparticles over the surface of nanoclay. The Fe_3O_4 nanoparticle peaks

didn't show any shifting of peaks supporting the fact that the loading of nanoparticle didn't involve any chemical bonding or structural changes within the nanoclay or nanoparticles. In XRD pattern of MnO_2/ Fe_3O_4/clay nanocomposite, appeared peaks match with the Fe_3O_4 XRD pattern, but the intensity of peaks is minimum, which is due to the fact that MnO_2 is distributed on Fe_3O_4/clay and hence effected the diffraction angle. The peaks of planes (300), (310), (131) are showing the successful adsorption of MnO_2 nanoparticles and (511) for iron oxide nanoparticles over the clay surface. In this case, peaks of both Fe_3O_4 and MnO_2 nanoparticles have appeared. Therefore, it can be concluded that both nanoparticles are assembled on nanoclay, as shown in Figure 4.3 (b). The XRD patern of nanocomposite did not show any shifting of peak encouraging the physical phenomenon for loading of nanoparticles

4.3. Fourier Transform Infrared Spectroscopy (FTIR)

For Fourier Transform Infrared Spectroscopy (FT-IR), powdered samples (as described above) of nanoparticles, nanoclay and nanocomposite were incorporated into a KBr pellets then spectra were calculated within range of 4000 cm^{-1} to 400 cm^{-1} wavenumbers. For FTIR spectroscopy, FT-IR spectrophotometer (PerkinElmer spectrum 100) was used.

4.3.1. FTIR of spectroscopy nanoparticles:

The Figure 4.4 (a) shows the FTIR spectrum of Fe_3O_4 and MnO_2 nanoparticles. The nanoparticles had intense peaks at 560 cm^{-1} and 521 cm^{-1} and a broad hump around 3500 cm^{-1}. The peaks at 560 cm^{-1} is because of the stretching vibrations of Fe-O bond with in the iron oxide nanoparticles whereas the peak at 521 cm^{-1} corresponds to the Mn-O bond. Broad hump at 3500cm^{-1} is due to hydroxyl groups stretching, hydroxyl groups are may be due to the absorption of moisture from atmosphere [68, 71-72]. It can be seen from figure that the synthesized nanoparticles don't have any impurity, as they have only peak of metal oxides

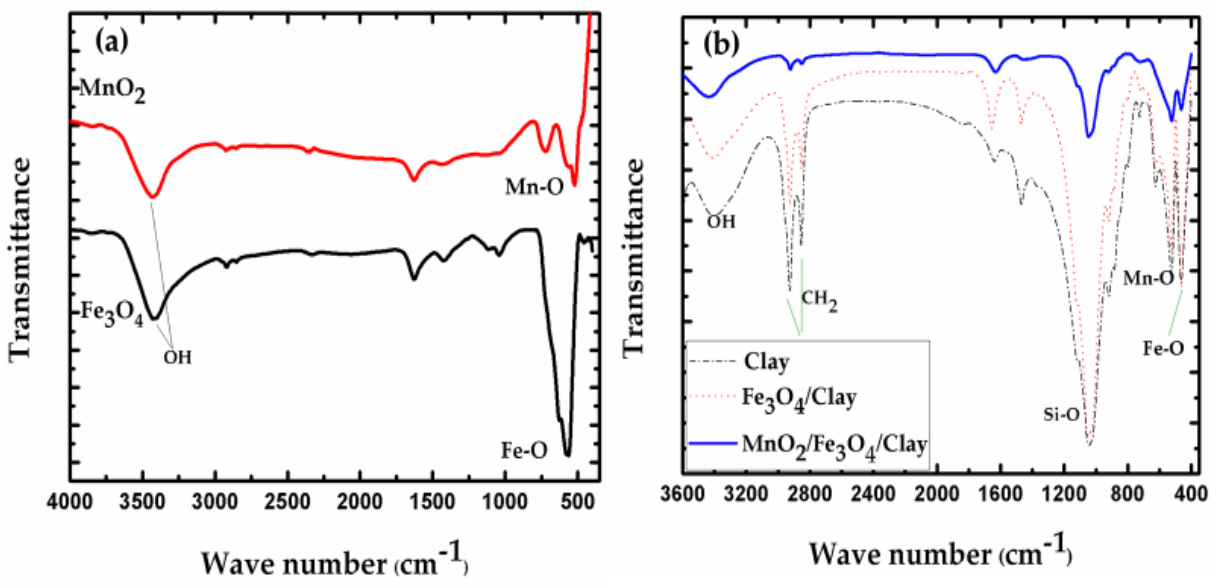

Fig. 4.4. FTIR spectrum of nanoparticles **(a)** and nanocomposites **(b)**.

4.3.2. FTIR spectroscopy of nanocomposites:

The broad peak at 3398.54 cm^{-1} in pure clay, Fe_3O_4/clay and MnO_2/Fe_3O_4/Clay nanocomposite is due to the presence of hydroxyl groups within the structure. As nanoclay has hydroxyl groups within the galleries and edges of the structure thus peak appeared due to stretching of OH bond, while the peaks at 2825.15 cm^{-1}, 2924.78 cm^{-1} supporting bending vibrations of C-H bonds in CH_2 groups respectively [69]. Clay structure also has some iron oxide and manganese groups within the layered structure and their peaks appear at 432 cm^{-1} and 521 cm^{-1}. For Fe_3O_4/Clay and MnO_2/Fe_3O_4/Clay nanocomposites intensities of the peaks at 432 cm^{-1} and 521 cm^{-1} increased due to the loading of nanoparticles. The peaks at the 1043.06 cm^{-1} and 1468 cm^{-1} are associated with the bending of Si-O groups also amine groups within nanoclay structure [70-71]. Appeared peaks didn't show any shifting or reduction in intensities, rather the intensities of Mn-O and Fe-O bond increased in case of nanocomposite. Therefore, it can be concluded that the nanocomposite synthesis didn't involve any significant chemical interactions and the adsorption of nanoparticles was due to the physical phenomenon. Figure 4.4 (b) showed the FTIR analysis of pure clay, Fe_3O_4/clay and MnO_2/Fe_3O_4/Clay nanocomposites.

4.4. UV-Vis Spectrophotometry

Samples for UV-Vis spectrophotometry were prepared in DI water for nanoparticles. The suspensions were 10^2 dilutions of 0.5 mg concentration of nanoparticles in 10ml, which were subsequently sonicated for 1.5 hour prior to testing. T-60 UV-Vis Spectrophotometer (PG Instruments), having wavelength sweep from 900 nm to 200 nm, was utilized for evaluating the absorbance data.

4.4.1. UV-Vis spectroscopy of nanoparticles:

The nanoparticles did not show any strong absorption in the visible region, supporting the inactive optical properties of nanoparticles in the visible region. In case of MnO_2 nanoparticles we found a hump in the region from 350-550nm, which is due to d-d orbital transition of Mn ion. This orbital transition showed splitting of d-energy level into higher and lower level because of octahedral arrangement of Mn and O [68-69] Figure 4.5 shows the optical behavior of MnO_2 and Fe_3O_4 nanoparticles.

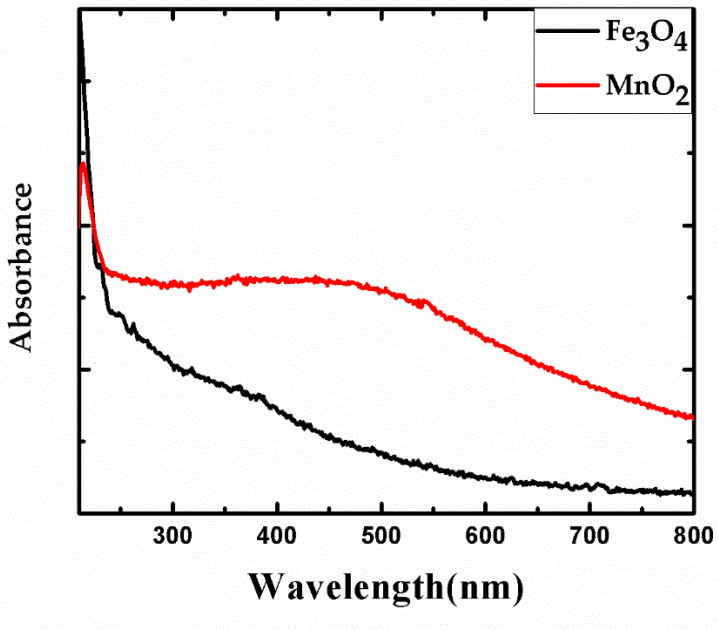

Fig. 4.5. UV-Vis Spectroscopy. Optical behavior of Fe_3O_4 and MnO_2 nanoparticles.

4.5. Adsorption studies of nanoparticles and nanocomposite:

Batch adsorption experiments were conducted to evaluate efficiency of metal removal using nanocomposites. Several parameters mainly varying pH, time of contact, initial concentration plus temperature for each experiment were examined. The adsorption capacities of materials at equilibrium is calculated by using the formula

$$Q_e=(c_i-c_e).v_o/m_o$$

Where q_e is the adsorption capacity at equilibrium, v_o is the initial volume of the solution(L), m_o is the amount of active material (g).

The sock solution of chromium was prepared as 1000 mg L^{-1} using potassium dichromate, which was subsequently adjusted to the desired concntration prior to utilize. For determination of adsorbed quantity per mass of adsorbent the nanoclay, MnO_2, and Fe_3O_4 NPs, MnO_2/Fe_3O_4/clay and Fe_3O_4/clay nanocomposite were developed as adsorbents for Cr^{6+} removal. A 0.05 g sample of the various materials were put into every 100 mL of solutions using initial concentration of $Cr6^+$ of 200 mg L^{-1} at a pH 2. The mixture was then shaked for 180 min at temperature (60 ^oC). The different phases were segregated using filter paper. In the subsequent experiments, MnO_2/Fe_3O_4/clay was chosen as the adsorbent and amount of adsorbent was remained constant. Adsorption capacity was examined by varying initial solution concentration from 50 mg/L to 300 mg/L. The impact of pH over Cr^{6+} adsorption was examined by changing the pH of solution from 2.0 to 5, with initial chromate concentration of 300 mg/L. Adsorption isotherms were produces by conducting the experiment at 295, and 335 K, using the sample solution having initial concentrations of 300 mg /L.

Adsorption kinetics of MnO_2/Fe_3O_4/clay was calculated using Cr^{6+} concentration as 50 mg L^{-1}, 100 mg $^{L-1}$, 200mg L^{-1}, 300 mg L $^{-1}$ at 60 ^oC. Samples were collected at fixed intervals utilizing filter paper.

4.5.1. Determination of Cr^{6+} concentration in the solution:

The concentration of chromate was calculated at wavelength of 540 nm. 0.2ml of the collected sampled was added into a few ml of water. Subsequently 0.5ml of 50% H_2SO_4 and H_3PO_4 was added as a buffer agent. 2ml of Diphenylcarbazied solution (250 mg in 50 ml of acetone) was used as a calorimetric agent. At the end 50 ml volume was adjusted by adding distilled water. The prepared solution was shaked and kept for 10 min before measurements.

4.5.2. Effect of variation in initial concentration of adsorbate on q_e:

4..5.2.1. Adsorption capacities of all materials:

The adsorption capacities of all materials, such as MnO_2, Fe_3O_4, nanoclay, Fe_3O_4/Clay, MnO_2/Fe_3O_4/Clay have been shown in Fig. 4.7. The sorption capacity of prepared MnO_2/Fe_3O_4/Clay nanocomposite showed excellent results towards chromium uptake than other materials. The experimental adsorption capacity for MnO_2/Fe_3O_4/Clay nanocomposite is 354.4 mg/g, Fe_3O_4/ clay is, Clay, Mno_2, Fe_3O_4 is 150 mg/g, 60 mg/g and 45 mg/g.

The adsorption capability of nanoclay is due to the surface groups mainly, C-H, OH present at the edges, capturing the metallic cations through cation exchange mechanism. The surface of nanoclay is negatively charged hence supports the adsorption of chromate ions. The adsorption of chromium ion by Fe_3O_4 and MnO_2 is due to their amphoteric behavior and affinity towards metal ions.

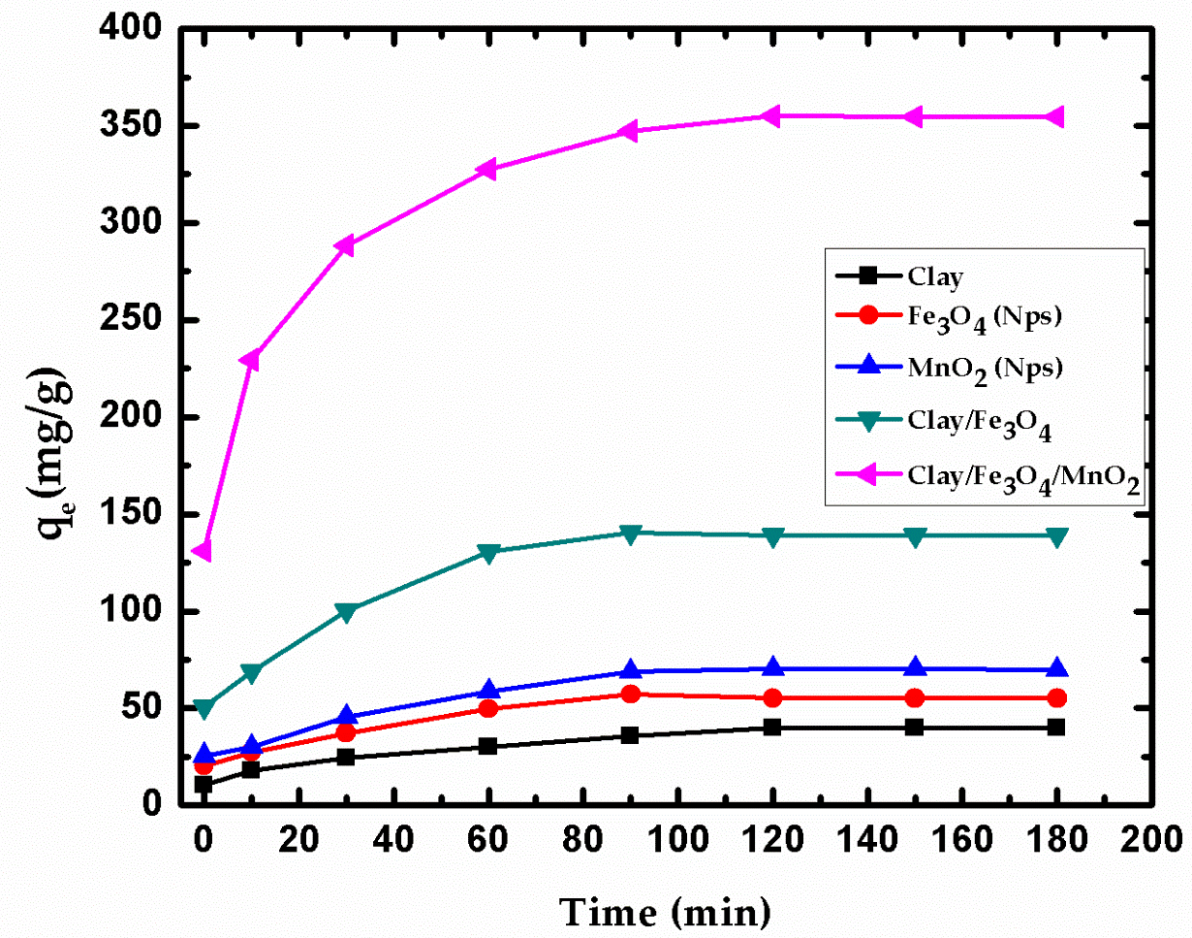

Fig.4.6: Adsorption Capacities of Different materials at same initial concentration of chromium

The increased adsorption capacity of Fe_3O_4/Clay composite is because of the combined sorption mechanism of nanoclay and magnetite nanoparticles, as seen in the SEM images that the Fe_3O_4 nanoparticles are uniformly distributed over nanoclay. Previously reported work showed that the adsorption capacities of pure nanoparticles are not enough, as they agglomerated in the solution lead to reduce their capturing activity [1]. Therefore, proper distribution of nanoparticles over supported structure is important for better results. Thus, higher surface area and chemical activity of nanoparticles increased the metal ions adsorption [1]. The adsorption capacity of MnO_2/Fe_3O_4/Clay is due to the combined effect of nanoparticles and nanoclay.

4.5.2.2. Adsorption capacity of MnO_2/Fe_3O_4/Clay nanocomposite:

The outstanding adsorption activity of MnO_2/Fe_3O_4/clay nanocomposite is due to the combined effect of both nanoparticles and nanoclay. Nanoclay and both nanoparticles capture the metallic cation through surface complexion and ion exchange mechanisms. The presence of groups mainly, Al-O, Si-O, CH_2, amine group and OH in clay structures support the adsorption mechanism. Pure clay showed adsorption activity due to its two-dimensional stacked structure having various charged groups within galleries for neutralization of structural charge [1]. Clay also have surfactant groups, which support the chromium uptake. Fe_3O_4 and MnO_2 nanoparticles, can sorb both negatively and positively charged specie, relying on pH. Fe_3O_4 would capture negatively charged Cr^{6+} specie in acidic medium by electrostatic interaction while MnO_2 nanoparticles can be protonated and deprotonated at varying pH and again adsorption is due to electrostatic attraction [70]. The adsorption of nanoparticles provided larger sorption sites while the morphology of nanoparticles influences the surface energy hence, chemical activity of the nanoparticles. Nanocomposite showed uniform dispersion of nanoparticles (having size less than 20 nm) without any agglomeration. Such arrangement of nanoparticles supports the capture of metallic species.

Literature showed that the sorption capacity of such kind of nanocomposite was improved due to the loading level of MnO_2 nanoparticles. Loading was successfully achieved without agglomeration in both kind of nanoparticles (as observed in SEM images). MnO_2/Fe_3O_4/clay give more active sites which is significant for the proper uptake of Cr^6+. Therefore, the sorption capabilities of various materials mainly influenced by the structure along with morphology of adsorbent.

In the Figure 4.8 the adsorption behavior of MnO_2/Fe_3O_4/Clay nanocomposite by varying initial solution concentration is shown. The adsorption phenomenon is because of the ion exchange, physiochemical interactions also surface complexation reactions. The adsorption capacities of nanocomposite increased by increasing the initial concentration of chromium. As in the case of varying solution concentration. The ratio of moles of solutes to available surface-active binding sites is low hence sorption depends upon the solute concentration within the bulk phase [1].

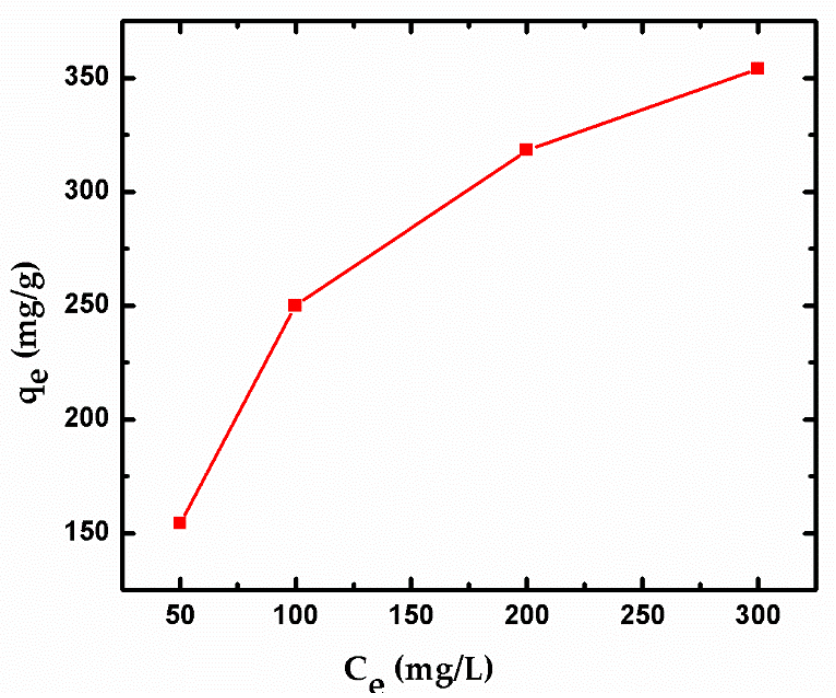

Fig. 4.7: Adsorption Capacity of Fe_3O_4/MnO_2/Clay at diff. initial concentration.

4.5.3. Effect of solution pH on adsorption capacity of MnO_2/Fe_3O_4/Clay composite:

Figure 4.8 is showing the adsorption capacities relative to initial pH of the solution. Initial pH of solution is the most important parameter for controlling the sorption phenomenon of chromium on the sorbent. pH of solution directly effects the chemical activities of metal ions, their oxidation state, surface of adsorbent and activity of adsorbent [78]. The adsorption capacity of chromium iron sharply decreases as pH increased from 3 to 5. This showed that the highly acidic medium is favorable for efficient removal of chromium. At lower pH, monovalent bichromate ($HCrO_4^-$) and divalent dichromate ($Cr_2O_7^{2-}$) specie are present but at higher pH the chromate ions (CrO_4^{2-}) have larger concentration. The binding energy of chromate ions is higher than that of monovalent bichromate ions. Moreover, lower pH provides larger quqntity of hydronium ions over the surface of sorbent and support the binding process of Cr^{6+} while at higher pH the

concentration of OH^- increases rather than hydronium ion due to the reduction of Cr(IV) into Cr^{3+}. The hydroxyl groups bind with the sorption site and reduce the metal sorption. Hence competitive adsorption starts between the divalent species (CrO_2^{-4} ($Cr_2O_2^{-7}$) and hydroxyl group. This whole mechanism showed decreasing trend of adsorption capacity at higher pH [70-71].

At lower pH, the surface of the nanoclay provides the charged ligand species which enhances the sorption of chromate ions. At lower pH the MnO_2 nanoparticles protonated into MnOH, while Cr^{6+} generally exist in the solution as cationic charge species, hence better sorption of chromium ions.

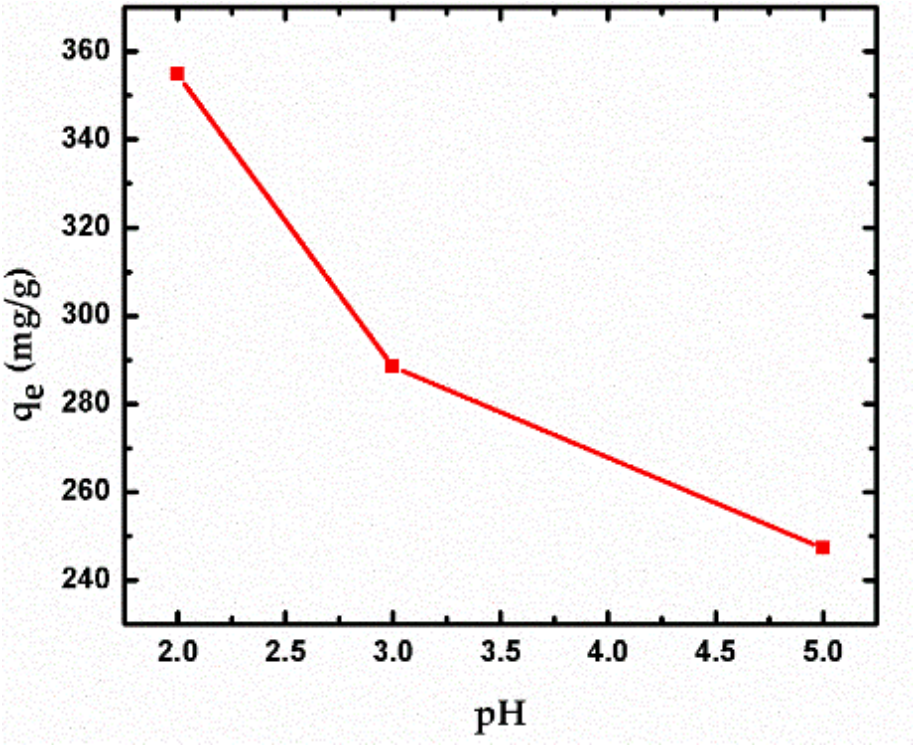

Fig. 4.8. Trend of adsorption capacity of MnO_2/Fe_3O_4/Clay nanocomposite at varying pH.

Figure. 4.9 showed the kinetics of whole adsorption mechanism at different pH. It can be seen that the adsorption capacity at every instant was decreased with the increase of pH. At higher pH, minimum adsorption capacity was observed.

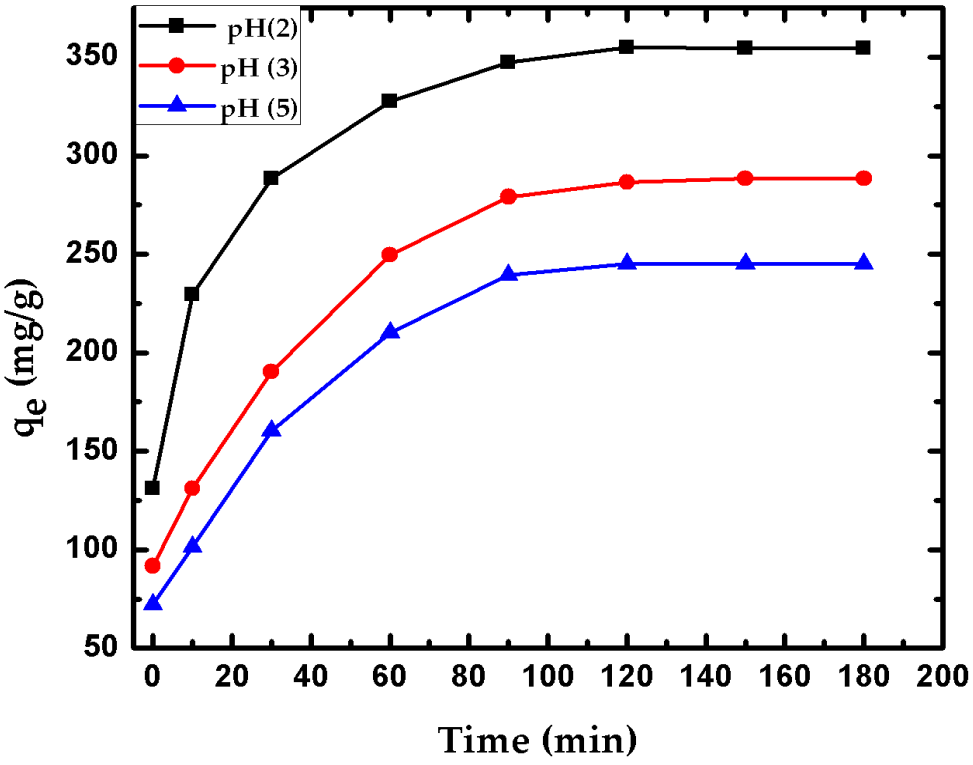

Fig. 4.9. Effect of pH over adsorption capacity of MnO_2/Fe_3O_4/Clay nanocomposite.

4.5.4. Effect of contact time on adsorption capacity of MnO_2/Fe_3O_4/Clay composite:

Contact time of sorption phenomenon gives information about the equilibrium between the adsorption and desorption of the metal species. At equilibrium in adsorption process further adsorption is not possible. The figure 4. 10 shows the affect of contact time on the sorption activity of nanocomposite.

Increased contact time, enhanced the sorption capacity of nanocomposite hence efficient removal of metal. In our case the removal of Cr^{6+} exhibited linear behavior with contact till it reached to

the equilbrium point. The impact of contact time was observed at different initial chromium solution concentration. The used concentration ranged from 50mg/L to 300 mg/L. The contact was established up to 180 min for each experiment to confirm the equilibrium point in adsorption process. The removal of metal showed similar behavior, equilibrium of adsorption was achieved at 120min in all cases. Increase in concentration has no effect on adsorption equilibrium. And after 120 min the adsorption alongwith desorption rate was equal. At initial stages of adsorption, the adsorption capacity was rapidly increasing but after 50 mins. the phenomenon was slowed down and achieved equilibrium at 120 mins. The calculated equilibrium capacity of nanocomposite at pH is 154.16, 250, 308.33, 354.12 mg g^{-1} for the 100, 200, and 300 mg L^{-1} initial $Cr6^{+}$ solution.

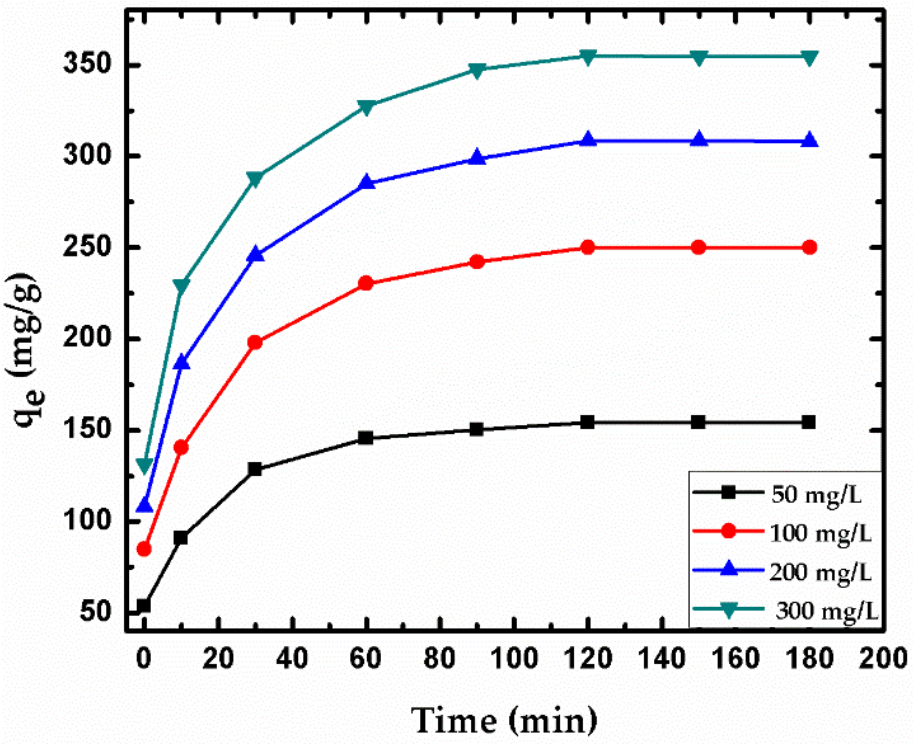

Figure 4.10: Effect of contact time on adsorption Capacity of Fe_3O_4/MnO_2/Clay at diff. initial concentrations

4.5.5. Adsorption isotherms study of MnO_2/Fe_3O_4/Clay composite:

Adsorption isotherm models are applied to the adsorption mechanism for evaluation of link between the adsorbed quantity of solute per unit mass of used adsorbent along with concentration of solute within the solution at operating temperature over equilibrium conditions. Using adsorption isotherm data, the impact of temperature over adsorption phenomenon can be accessed. Hence it is necessary to establish the most suitable relationships for batch equilibrium statistics with empirical or theoretical calculations [1, 23]. Adsorption data was examined by Langmuir and Freundlich isotherm models. Such models are used for analyzing solid–liquid sorption behavior. The first model uses some assumptions, likely adsorption will be localized, adsorption mechanism is analogous at active site of surface, binding sites will share same energies over surface and interaction between the adsorbate is negligible. This model is expressed as follows [24-25];

$$\mathbf{C_e/q_e=1/bq_m + Ce/q_m}$$

while q_e (mg/g) is the amount of adsorbate adsorbed per unit weight of the adsorbent, C_e (mg/L) is the concentration of adsorbate over equilibrium, q_m (mg g^{-1}) is the optimum amount of adsorbing species that creates a complete monolayer over surface, lastly, b (L mg^{-1}) is the Langmuir constant denoting adsorption heat.

The Freundlich isotherm model describes non-ideal adsorption mechanism and suitable for nonuniform surface, adsorption occurring in multilayered pattern and nonhomogeneous distribution of energy with affinity over active sites. This model is represented as follows [24]:

$$\mathbf{\ln q_e = \ln K_F + 1/n \ln C_e}$$

Table 4.1 showed the results of both applied models. Experimental results fitted well with Langmuir isotherm with appropriate correlation coefficients. The data showed equal distribution of energies of binding sites over surface of nanocomposite, while interaction between the adsorbed molecule was minimum. The maximum adsorption capacity of Cr^{6+} was improved

from 263 mg/g to 384 mg/g due to the rise in temperature from 295 K to 335 K. increase in sorption capacity with temperature representing the probability of endothermic process for Cr^{6+} adsorption.

Temp.(K)	**Langmuir isotherm**				**Freundlich isotherm**		
	q_e (mg g^1)	**B**	**r^2_1**	**R_L**	**1/n**	**k_f**	**r_2^2**
295	263	0.022	0.9998	0.135-0.47	0.3645	31.689	0.9718
335	384	0.0449	0.996	0.07-0.308	0.2858	78.507	0.9617

Table 4.1: Adsorption isotherms of MnO_2/Fe_3O_4/Clay at diff. temperature

Table 1 shows the evaluated Rl values contrasted with initial Cr^{6+} concentration on 295, and 335K. The R_L values are in the 0–1 range, whih specifies the aptness of MnO_2/Fe_3O_4/clay nanocomposite as Cr^{6+} adsorbent.

4.5.6. Adsorption kinetics of MnO_2/Fe_3O_4/Clay composite:

The influence of contact time at the adsorption capacity, reaction pathways and mechanism of adsorption is explained by studying the reaction kinetics. Several models were defined for analysis of adsorption kinetics and reaction mechanism mainly zero, first, second, third order, pseudo first, second order, Intraparticle diffusion, Elovich and the first order reversible. But the most frequently used model is the pseudo- second order kinetic model having linear form as follows [23];

$$q_t = 1/kq^2_e + t/q_e$$

where q_e and q_t is the adsorption capabilities at equilibrium and at time t (min), k (g mg^{-1} min^{-1}) is the adsorption constants of pseudo-second order kinetics equation. The linear plot of 1/ (q_e–q_t)

versus t expresses the kinetic model. Initial adsorption rate h (mg/ g min) is evaluated using pseuodo second order rate as follows [71];

$$\mathbf{h = kq_e^2}$$

C_0 (mg l^{-1})	q_e, exp	Pseudo-second-order kinetic model			
		$k(10^{-4})$	q_e	h	R
50	154	14.1	158	44.49	0.9988
100	250	6.79	256	34	0.9981
200	308	5.78	320	60.23	0.9984
300	354	5.74	370	78.58	0.9987

Table 4.2: The kinetic parameter and associated coefficient of Cr^{6+} at different initial concentration are presented.

The adsorption capacities that are calculated using kinetic model is shown as qe and have values (50mg L^{-1}; 158 mg/g, 100 mg /L; 256 mg g^{-1}, 200 mg L^{-1}; 320mg g^{-1}, also 300 mg L^{-1};
370mg g^{-1}) larger than experimental values. The values of 'r' are close to 1, showing the aptness of pseudo-second-order model for our adsorption process. The calculated and experimental adsorption capacities have small difference; hence it can be said that the sorption process can explained efficiently using the pseudo-second-order model. The rate constants were not so large, showing that the adsorption process was not so quick. At start the adsorption process was fast but soon it became slower until reached to the equilibrium. The initial rate of sorption increased by the increase of initial Cr^{6+} conc.

The overall rate of sorption process can be regulated by means of external mass transfer, chemical also physical adsorption mechanism. The process of adsorption using kinetic model,

was defined as impulsive plus endothermic. In this case the sites for adsorption activities are almost equal to square of unoccupied sites.

Conclusions

MnO_2 and Fe_3O_4 NPs and their nanocomposites were successfully synthesized, characterized and used for the adsorption studies to remove chromate ion from aqueous system. The prepared nanocomposite is of Cloisite 30-B nanoclay decorated with the iron oxide and manganese oxide nanoparticles. In nanocomposites, spherical shaped NPs were homogeneously dispersed on the surface of the clay which supported enhanced adsorption of species due to enhanced surface area. Several characterization techniques have been utilized mainly X-Ray diffraction, scanning electron microscopy, Fourier transform infrared spectroscopy, UV-Vis spectroscopy for analysis of synthesized materials.

MnO_2/Fe_3O_4/Clay nanocomposite has been demonstrated to be the excellent adsorbent for the chromium ions removal. It has also been demonstrated that by increasing pH the adsorption capacity decreased. For MnO_2/Fe_3O_4/Clay nanocomposite, the maximum adsorption capacity evaluated using Langmuir isotherm was found to be 384 mg g^{-1} at 335K. The kinetic data was found to fit with pseudo second order kinetic model where the initial adsorption rate was found to increase due to increase in the initial solution concentration. The adsorption process was found to be physio-chemical. The adsorption capacity of MnO_2/Fe_3O_4/Clay nanocomposite was demonstrated to be depended on the structure, morphology, surface area, presence of functional groups on the adsorbent as well as on the pH and temperature of the system. Due to availability and low cost of the nanoclay in comparison to other adsorbents such as graphene, graphene oxides, conducting polymers and MWCNTs, MnO_2/Fe_3O_4/Clay nanocomposite shows great promise as adsorbent for the removal of heavy metal ions from aqueous system.

References

[1] Sanjay K. Sharma, Heavy Metals in Water Presence, Removal and Safety, Royal society of chemistry, 2015.

[2] Fenglian Fu, Qi Wang, Removal of heavy metal ions from wastewaters, Journal of Environmental Management, 92 **(2011)** 407-418.

[3] Manju Bhargavi Gumpu, Swaminathan Sethuraman, Uma Maheswari Krishnan, John Bosco Balaguru Rayappan, A Review on Detection of Heavy Metal Ions In Water –An Electrochemical Approach, Sensors and Actuators B, 213**(2015)** 515-533.

[4] H.B. Bradl, Heavy Metals in the Environment: Origin, Interaction and Remediation, Interface Science and Technology; 2005.

[5] Barrera-Díaz, Violeta Lugo-Lugoa,b, Bryan Bilyeu, A review of chemical, electrochemical and biological methods for aqueous Cr(VI) reduction, Journal of Hazard Mater, (**2012**) 223-224.

[6] Yan Wu, Hanjin Luo, Hou Wang, Can Wang, Jian Zhang, Zilong Zhang, Adsorption of hexavalent chromium from aqueous solutions by graphene modified with cetyltrimethylammonium bromide, Journal of Colloid and Interface Science, 394**(2013)** 183-191.

[7] Yan Liu, Chao Luo*a*, Guijia Cui, Shiqiang Yan, Synthesis of manganese dioxide/iron oxide/graphene oxide magnetic nanocomposites for hexavalent chromium removal, RSC Advances, 67 (**2015)** 54156-54164.

[8] Lin Cui, Jie Wu, Huangxian Ju, Electrochemical sensing of heavy metal ions with inorganic, organic and bio-materials, Biosensors and Bioelectronics 63 **(2015)** 276–286.

[9] Guo Jian-feng, Hou Chang-jun, Yang Mei, Huo Dan-qun, Li Jun-jie, Fa Huan-bao, Luo Hui-bo, Yang Ping, Colorimetric sensing of chromium(VI) ions in aqueous solution based on the leaching of protein-stabled gold nanoparticles, Journal of Analytical Methods, 27**(2016)** 5526-5532.

[10] ChanilJung, Jiyong, Heo,Jonghun Han, Nam guk Her,Sung Jae Lee, Jeill Oh,Jaena Ryu,YeominYoon, Hexavalent chromium removal by various adsorbents: Powdered activated carbon, chitosan, and single/multi-walled carbon nanotubes.

[11] Natural Clay Minerals as Environmental Cleaning Agents.

[12] Maryam Fayazi, Mohammad Ali Taher, Daryoush Afzali, Ali Mostafavi, Fe3O4 and MnO2 assembled on halloysite nanotubes: A highly efficient solid-phase extractant for electrochemical detection of mercury(II) ions, Sensors and Actuators B: Chemical, 228 (2016) 1–9

[13] Wei Ye, Binxia, Zhao, Han Gao, Jiajun Huang, Xiaoli Zhang, Preparation of highly efficient and stable Fe, Zn,Al-pillared montmorillonite as heterogeneous catalyst for catalytic wet peroxide oxidation of Orange II, 23**(2016)**301–310.

[14] Lee Blaney, Magnetite (Fe3O4): Properties, Synthesis, and Applications, Lehigh Preserve, 15(2017).

[15] J.M.D Coey, Magnetism and Magnetic Materials, Cambridge University Press; 2009.

[16] N.A. Spaldin, Magnetic materials: fundamentals and applications: Cambridge University Press; 2010.

[17] Muhammad Shahid Nazir, Mohamad Haafiz, Mohamad Kassim, Lagnamayee Mohapatra, Mazhar Amjad Gilani, Muhammad Rafi Raza, Khaliq Majeed, Characteristic Properties of Nanoclays and Characterization of Nanoparticulates and Nanocomposites, Nanoclay Reinforced Polymer Composites, **(2016)**35-55.

[18] Clays, Nanoclays, and Montmorillonite Minerals, Metallurgical and Materials Transactions A, 39 **(2008)** 2804-2814.

[19] David M. Robinson, Yong Bok Go, Michelle Mui, Graeme Gardner, Zhijuan Zhang, Daniel Mastrogiovanni, Eric Garfunkel, Jing Li, Martha Greenblatt and G. Charles Dismukes, Photochemical Water Oxidation by Crystalline Polymorphs of Manganese Oxides: Structural Requirements for Catalysis, J. Am. Chem. Soc., (**2013)**135, 3494−3501.

[20] S. Devaraj and N. Munichandraiah, Effect of Crystallographic Structure of MnO2 on Its Electrochemical Capacitance Properties, J. Phys. Chem. C, (**2008**)112, 4406-4417.

[21] Insight into the adsorption kinetics models for the removal of contaminants from aqueous solutions K.L. Tan, B.H. Hameed, Journal of the Taiwan Institute of Chemical Engineers, (2017) 1–24.

[22] Patiha, E Heraldy, Y Hidayat, M Firdaus, The langmuir isotherm adsorption equation: The monolayer approach, Materials Science and Engineering, 107**(2016)** 012067.

[23] L. Largitte, R. Pasquier, New models for kinetics and equilibrium homogeneous adsorption, chemical engineering research and design, 112 **(2016)** 289–297.

[24] Brian Bolto, David Dixon, Rob Eldridge, Simon King, Cationic Polymer and Clay or Metal Oxide Combinations for Natural Organic Matter Removal, Water Resources, 35**(2001)** 2669-76.

[25] Achyut K. Pandaa, B.G. Mishraa, D.K. Mishrac, R.K. Sing**,** Effect of sulphuric acid treatment on the physico-chemical characteristics of kaolin clay colloids and Surfaces A,363(2010) 98-104.

[26] Sabriye Yusan, Cem Gok, Sema Erenturk, Sule Ayta, Adsorptive removal of thorium (IV) using calcined and flux calcined diatomite from Turkey: Evaluation of equilibrium, kinetic and thermodynamic data Applied Clay Science, 67–68, (2012)106-116.

[27] Wenji Wang, Hao Chen, Aiqin Wang, Adsorption characteristics of Cd(II) from aqueous solution onto activated palygorskite, Separation and Purification Technology, 55(2007)157-164

[28] O. Abollinoa, M. Acetob, M. Malandrinoa, C. Sarzaninia, E. Mentasti, Adsorption of heavy metals on Na-montmorillonite. Effect of pH and organic substances, Water Research, 37 (2003) 1619-1627.

[29] John U. Kennedy Oubagaranadin, Zagabathuni, V.P. Murthy, Veeresh P. Mallapur, Removal of Cu(II) and Zn(II) from industrial wastewater by acid-activated montmorillonite-illite type of clay, Comptes Rendus Chimie,13(2010)1359-1363.

[30] T.S. Anirudhan, S. Jalajamony, S.S. Sreekumari, Adsorption of heavy metal ions from aqueous solutions by amine and carboxylate functionalised bentonites, Applied Clay Science, 65–66(2012)67-71.

[31] Mabrouk Eloussaief, Ikram Jarraya, Mourad Benzina, Adsorption of copper ions on two clays from Tunisia: pH and temperature effects, Applied Clay Science, 46 (2009) 409-413.

[32] Susmita Sen Gupta, Krishna G. Bhattacharyya, Removal of Cd(II) from aqueous solution by kaolinite, montmorillonite and their poly(oxo zirconium) and tetrabutylammonium derivatives, Journal of Hazardous Materials, 128(2006) 247-25.

[33] Mabrouk Eloussaief , Mourad Benzina, Efficiency of natural and acid-activated clays in the removal of Pb(II) from aqueous solutions, Journal of Hazardous Materials,178(2010)753-757.

[34] Ageetha Vanamudan, Padmaja Pamidimukkala, Chitosan, nanoclay and chitosan–nanoclay composite as adsorbents for Rhodamine-6G and the resulting optical properties international, Journal of Biological Macromolecules, 74(2015) 127-135.

[35] Dong-Wan Cho, Byong-Hun Jeon, Chul-Min Chon, Yongje Kim, Franklin W. Schwartz, Eung-Seok Lee, Hocheol Song, A novel chitosan/clay/magnetite composite for adsorption of Cu(II) and As(V), Chemical Engineering Journal, 202 (2012) 654-662.

[36] Daimei Chen, Wa Li, Yanru Wu, Qian Zhu, Zhijin Lu, Gaoxiang Du, Preparation and characterization of chitosan/montmorillonite magnetic microspheres and its application for the removal of Cr (VI), Chemical Engineering Journal, 221**(2013**)8-15.

[37] Manpreet Kaur, Mandeep Singh, Siddharth Shankar Mukhopadhyay, Dhanwinder Singh, Munish Gupta, Structural, magnetic and adsorptive properties of clay ferrite nanocomposite and its use for effective removal of Cr (VI) from water, Journal of Alloys and Compounds,653**(2015)** 202-211.

[38] Mohammad Kashif Uddin, A review on the adsorption of heavy metals by clay minerals, with special focus on the past decade, Chemical Engineering Journal, 308**(2017)** 438-462.

[39] Maisa A. Moreira, Katia J. Ciuffi, Vicente Rives, Miguel A. Vicente, Raquel Trujillano, Antonio Gil, Sophia A. Korili, Emerson H. de Faria, Effect of chemical modification of palygorskite and sepiolite by 3-aminopropyltriethoxisilane on adsorption of cationic and anionic dyes, Applied Clay Science,135**(2017)**394-404.

[40] Nilesh B. Shrigadi, Ajit B. Shinde, Shriniwas D. Samant, Study of catalytic activity of free and K10-supported iron oxyhydroxides and oxides in the Friedel–Crafts benzylation reaction using benzyl chloride/alcohol to understand their role in the catalysis by the Fe-exchanged/impregnated K10 catalysts, Applied Catalysis A, 252**(2003)**23-35.

[41] Sílvia C.R. Santos, Rui A.R. Boaventura, Adsorption of cationic and anionic azo dyes on sepiolite clay: equilibrium and kinetic studies in batch mode Journal of Environmental Chemical Engineering, 4(2016)1473-1483.

[42] Manpreet Kaur, Mandeep Singh, Siddharth Shankar Mukhopadhyay, Dhanwinder Singh, Munish Gupta, Structural, magnetic and adsorptive properties of Clay ferrite nanocomposite and its use for effective removal of Cr (VI) from water, Journal of Alloys and Compounds, 653 (2015) 202-211.

[43] M. Soleimani, Z. Hassanzadeh Siahpoosh, Determination of Cu(II) in water and food samples by Na+-cloisite nanoclay as a new adsorbent: Equilibrium, kinetic and thermodynamic studies, Journal of the Taiwan Institute of Chemical Engineers, 59**(2016)** 413-423.

[44] Shadpour Mallakpour, Samira Moslemi, Dispersion of chiral amino acid organomodified Cloisite Na+ in poly(vinyl alcohol) matrix for designing of novel bionanocomposite films, Progress in Organic Coatings,74(2012) 8-13.

[45] AgeethaVanaamudan, Padmaja P.Sudhakar, Equilibrium, kinetics and thermodynamic study on adsorption of reactive blue-21 and reactive red-141 by chitosan-organically modified nanoclay (Cloisite 30B) nano-bio composite, Journal of the Taiwan Institute of Chemical Engineers, 55(2015)145-151.

[46] Ali Ammar, Ahmed Elzatahry , Mariam Al-Maadeed, Abdullah M. Alenizi, Abul F. Huq, Alamgir Karim, Nanoclay compatibilization of phase separated polysulfone/polyimide films for oxygen barrier, Applied Clay Science, 137(2017) 123-134.

[47] Sadanand Pandey, Shivani B. Mishra, Organic–inorganic hybrid of chitosan/organoclay bionanocomposites for hexavalent chromium uptake, Journal of Colloid and Interface Science, 361(2011)509-520.

[48] Luiz C.A. Oliveiraa, Rachel V.R.A. Rios a , Jose´ D. Fabrisa, Karim Sapagb, Vijayendra K. Gargc, Rochel M. Lago, Clay–iron oxide magnetic composites for the adsorption of contaminants in water, Applied Clay Science, 22(2003)169-177.

[49] Vijaya kumar Badathala, Justin Ponniah, MnO2/mont K10 composite for high electrochemical capacitive energy storage, International Journal of Hydrogen Energy, 41(2016)12183-12193**.**

[50] J.Praveen Kumar, P.V.R.K. Ramacharyulu, G.K. Prasad, Beer Singh, Montmorillonites supported with metal oxide nanoparticles for decontamination of sulfur mustard, Applied Clay Science,117(2015) 263-272.

[51] Peng Yuan, Dong Liu, Ming deFan, DanYang, Runliang Zhu, FeiGe, Jian XiZhu, Hongping He, Removal of hexavalent chromium [Cr(VI)] from aqueous solutions by the diatomite-supported/unsupported magnetite nanoparticles, Journal of Hazardous Materials, 173**(2010)** 614-621.

[52] annamária mockovčiaková, mária orolínová, zuzana danková Cd(ii) adsorption by magnetic clay composite under the ultrasound irradiation, Energy and Environmental Engineering, 1(**2013)**74-80.

[53] Xiaoyao Guo, Bin Du, Qin Wei, Jian Yang, Lihua Hu, Liangguo Yan, Weiying Xu, Synthesis of amino functionalized magnetic graphenes composite material and its application to remove Cr(VI), Pb(II), Hg(II), Cd(II) and Ni(II) from contaminated water Journal of Hazardous Materials, 278(**2014)** 211-220.

[54] Guohong Qiu, Hui Huang, Saminda Dharmarathna, Evan Benbow, Lisa Stafford, Steven L. Suib, Hydrothermal Synthesis of Manganese Oxide Nanomaterials and Their Catalytic and Electrochemical Properties, *Chem. Mater.*, 23**(2011)** 3892–3901.

[55] Mohammad Mahdi Najafpour, Foad Ebrahimi, Mahnaz Abasi, Małgorzata Hołynska, Seyedeh Maedeh Hosseini, Manganese oxides supported on nano-sized metal oxides as water oxidizing catalysts for water splitting systems: 1-synthesis and characterization

[56] synthesis of Fe3O4 nps

[57] Liang Chena, Li-Jie Suna, Feng Luana, Ying Lianga, Yat Li, Xiao-Xia Liua, Synthesis and pseudocapacitive studies of composite films of polyaniline and manganese oxide nanoparticles, Journal of Power Sources, 195 **(2010)** 3742–3747.

[58] Peng Yuan, Mingde Fan, Dan Yang, Hongping He, Dong Liu, Aihua Yuan, JianXi Zhu, TianHu Chen, Montmorillonite-supported magnetite nanoparticles for the removal of hexavalent chromium [Cr(VI)] from aqueous solutions, Journal of Hazardous Materials 166 **(2009)** 821–829.

[59] Shaojun Yao, Shuai Yuan, Junhui Xu, Ying wang, Jianlin Luo, Shengshui Hu, A hydrogen peroxide sensor based on colloidal MnO2/Na-montmorillonite, Applied Clay Science 33 **(2006)** 35–42.

[60] Elton N. Kaufmann, CHARACTERIZATION OF MATERIALS, John Wiley and Sons Publication, 2003.

[61] B S Murty, P Shankar, Baldev Raj, B B Rath, James Murday, Nanoscience and Nanotechnology, spriner 2013.

[62] Zhen Guo, Li Tan, Fundamentals and Applications of Nanomaterials, ARTECH HOUSE, 2009.

[63] William D. Callister, Jr., Materials Science and Engineering; An Introduction, John Wiley & Sons, 2007

[64] B. M. Weckhuysen, In-situ Spectroscopy of Catalysts, American Scientific Publishers, 2004.

[65] Douglas A. Skoog, Donald, M. West, F. James Holler, Stanley R. Crouch, Fundamentals of Analytical Chemistry, 2014, Brooks/Cole, Cengage Learning.

[66] Charles P. Poole, Jr., Frank J. Owens, Introduction to Nanotechnology, John Wiley & Sons, 2003.

[67] V. S. Bagotsky, Fundamentals of Electrochemistry, John Wiley & Sons, 2006.

[68] Mokae fanuel Bambo, Rui werner marcedo Krause, Richard Motlhaletsi Moutloali, Facile Method for Synthesis of Copper nanoparticles supported on Organoclay materials, Journal of Biomaterials and nanobiotechnology, 8 **(2017)**, 144-158.

[69] H, Assaedi, F. U. A. Shaikh, I.M. lo, Effect of nanoclay on mechanical and thermal properties of geopolymer, Journal of assian ceramics societies, 140, (**2015).**

[70] Yen Pin Yew, Kamyar Shameli, Mikio Miyake, Noriyuki Kuwano, Nurul Bahiyah Bt Ahmad Khairudin, Shaza Eva Bt Mohamad, Kar Xin Lee, Green Synthesis of Magnetite (Fe3O4) Nanoparticles Using Seaweed (Kappaphycus alvarezii) Extract, Nanoscale Research Letters, 11 **(2016**), 276.

[71] Anbao Yuan, Qinglin Zhang, A novel hybrid manganese dioxide/activated carbon supercapacitor using lithium hydroxide electrolyte, Electrochemistry Communications, 8 **(2006)**, 1173–1178.